AGU PUBLICATIONS

Water Resources Research

RESEARCH ARTICLE
10.1002/2014WR016719

The spatial and temporal evolution of contributing areas

Fabian Nippgen[1,2], Brian L. McGlynn[1], and Ryan E. Emanuel[3]

[1]Nicholas School of the Environment, Department of Earth and Ocean Sciences, Duke University, Durham, North Carolina, USA, [2]Department of Land Resources and Environmental Sciences, Montana State University, Bozeman, Montana, USA, [3]Department of Forestry and Environmental Resources, North Carolina State University, Raleigh, North Carolina, USA

Key Points:
- Storage patterns determined by lateral water redistribution and ET
- Streamflow driven by storage threshold-mediated connectivity
- Contributing areas show hysteretic behavior with streamflow

Correspondence to:
F. Nippgen,
fabian.nippgen@duke.edu

Citation:
Nippgen, F., B. L. McGlynn, and R. E. Emanuel (2015), The spatial and temporal evolution of contributing areas, *Water Resour. Res.*, *51*, 4550–4573, doi:10.1002/2014WR016719.

Received 3 DEC 2014
Accepted 8 MAY 2015
Accepted article online 12 MAY 2015
Published online 25 JUN 2015

Abstract Predicting runoff source areas and how they change through time is a challenge in hydrology. Topographically induced lateral water redistribution and water removal through evapotranspiration lead to spatially and temporally variable patterns of watershed water storage. These dynamic storage patterns combined with threshold mediation of saturated subsurface throughflow lead to runoff source areas that are dynamic through time. To investigate these processes and their manifestation in watershed runoff, we developed and applied a parsimonious but spatially distributed model (WECOH—Watershed ECOHydrology). Evapotranspiration was measured via an eddy-covariance tower located within the catchment and disaggregated as a function of vegetation structure. This modeling approach reproduced the stream hydrograph well and was internally consistent with observed watershed runoff patterns and behavior. We further examined the spatial patterns of water storage and their evolution through time by building on past research focused on landscape hydrologic connectivity. The percentage of landscape area connected to the stream network ranged from less than 1% during the fall and winter base flow period to 71% during snowmelt. Over the course of the 2 year study period, 90% of the watershed areas were connected to the stream network for at least 1 day, leaving 10% of area that never became connected. Runoff source areas during the event shifted from riparian dominated runoff to areas at greater distances from the stream network when hillslopes became connected. Our modeling approach elucidates and enables quantification and prediction of watershed active areas and those active areas connected to the stream network through time.

1. Introduction

Efforts to trace watershed runoff to its source areas and to determine how much of a watershed contributes to (storm-)runoff have been a central focus of watershed hydrology for many decades. While early studies still emphasized Hortonian, i.e., infiltration excess, surface runoff [e.g., *Betson*, 1964; *Ragan*, 1968; *Dickinson and Whiteley*, 1970], a paradigm shift occurred with recognition that runoff—both during and between storms—can be largely generated in the subsurface [e.g., *Hewlett and Hibbert*, 1963; *Tsukamoto*, 1963]. This lead to the formulation of the variable source area (VSA) concept, which states that storm runoff is mainly generated by subsurface flow in expanding and contracting near-stream areas [*Hewlett and Hibbert*, 1967]. Variations of the variable source area concept that included saturation excess overland flow from near-stream areas were formulated by *Dunne and Black* [1970]. The variable source area concept also formed the core of one of the more popular research-oriented hydrologic models to date, TOPMODEL [*Beven and Kirkby*, 1979]. A commonality across these studies and concepts was that even during intense storms only a fraction of the watershed delivered water to the stream network.

Knowledge of runoff generation mechanisms advanced further with studies recognizing that source areas were not limited to lower hillslopes and near-stream areas, but that flow in the subsurface largely via preferential flow pathways extending up the hillslope contributed to watershed runoff [e.g., *Mosley*, 1979; *McDonnell*, 1990; *Woods and Rowe*, 1996]. Subsequent studies [e.g., *McGlynn and McDonnell*, 2003a, 2003b] further documented that the threshold-mediated establishment of shallow water tables on hillslopes essentially created a hydrologic connection between the watershed uplands and the stream network. *McGlynn and McDonnell* [2003b], for example, explained changes in dissolved organic carbon during runoff events with a shift in runoff source areas from riparian (the classic variable source areas) to hillslopes, after the hillslopes exceeded a moisture-based threshold and became hydrologically connected to the stream network. As such, this watershed connectivity can be viewed as an extension of the classic variable source area concept,

© 2015. American Geophysical Union. All Rights Reserved.

while including individual landscape elements (e.g., hillslopes) to the source areas without the restriction to specific runoff generation processes. Forty years ago, John Hewlett published a comment in *Water Resources Research* defending and further defining the concept of variable source areas [*Hewlett*, 1974]. This was before research had fully emphasized macropore flow, perched shallow groundwater flow, and other preferential runoff generation mechanisms. However, in *Hewlett*'s [1974] definition, "subsurface stormflow is any water passing the gaging station that has, however briefly, entered the mineral soil surface and has traveled for some distance, however short, within the soil." This definition allows incorporation of many—if not all—runoff generation mechanisms under the umbrella of the variable (or contributing) source area and helps to define hydrologic connectivity.

Factors leading to the formation of a hydrologic connection and the duration thereof have previously been attributed to (variations in) topography [e.g., *Sidle et al*., 1995; *McGlynn and McDonnell*, 2003b; *Jencso et al*., 2009], soil properties [e.g., *Buttle and McDonald*, 2002], and soil type [e.g., *Tetzlaff et al*., 2007], as well as variability in vegetation cover [e.g., *Hwang et al*., 2012; *Emanuel et al*., 2014]. Furthermore, the establishment of lateral (subsurface) flow exhibits threshold behavior [e.g., *Sidle et al*., 2000; *McGlynn and McDonnell*, 2003a; *Tromp-van Meerveld and McDonnell*, 2006b; *Lehmann et al*., 2007; *Penna et al*., 2011], where either the exceedance of rainfall depths/intensities or soil moisture states ultimately lead to a response (e.g., activation of a flow pathway) or to a response disproportionately greater than below those thresholds. However, determining thresholds a priori can be a challenge because there is no singular precipitation threshold for hillslopes (e.g., *Weiler et al*. [2006] or *Ali et al*. [2013]).

Despite marked progress in identifying the mechanisms leading to the activation of flow paths, the detection and prediction of areas contributing water to the stream network remains a challenge. The difference between "active" and "contributing" areas further complicates this assessment. The terms "active" and "contributing" are often used interchangeably especially in reference to the VSA concept. However, as *Ambroise* [2004] points out, "active" areas are not necessarily "contributing" areas. *Ambroise* [2004] suggests that "contributing" be used for areas that have an established hydraulic connection to the stream network, while fluxes in "active" areas may be isolated from the stream network and not contribute to watershed runoff when the downhill flow paths are discontinuous.

Fully distributed watershed models capable of tracking runoff source areas—or contributing areas—are often data intensive and include numerous parameters (e.g., DHSVM [*Wigmosta et al*., 1994], RHESSys [*Band*, 1993], and PIHM [*Qu and Duffy*, 2007]), which could increase the degree of equifinality [*Beven*, 2006] and may lead to various representations of internal system behavior [*Kelleher et al*., 2015]. Here we present a parsimonious but fully distributed modeling framework that incorporates topographically driven lateral water redistribution and eddy covariance derived spatially disaggregated evapotranspiration measurements to simulate streamflow and the spatial distribution of water stored in the watershed through time. The goal of the model development and this particular application was to inform our understanding of the spatial and temporal dynamics of runoff source areas. Utilizing and testing this diagnostic modeling framework in conjunction with empirical measurements of hillslope connectivity through an extensive network of shallow groundwater wells [*Jencso et al*., 2009, 2010; *Jencso and McGlynn*, 2011], we approximated watershed connectivity to investigate how runoff source areas change in space and time over the course of two water years in a snowmelt dominated system.

2. Methods

2.1. Site Description

The Tenderfoot Creek Experimental Forest (TCEF) is located in the Little Belt Mountains in the Rocky Mountains of central Montana (latitude 56.55′N, longitude 110.52′W). The total area of TCEF encompasses 2300 ha. Tenderfoot Creek is a tributary of the Smith River, which drains into the Missouri. For this study, we focused on the 555 ha (5.55 km^2) Lower Stringer Creek (LSC) subwatershed (Figure 1). The elevation in LSC ranges from 1992 to 2426 m, which is also the highest elevation in TCEF. Slope in LSC increases in downstream direction, while the riparian areas (~2% of total area) get narrower and more constrained toward the outlet. Extensive park areas occur mainly in the upper parts of the watershed.

Lodgepole Pine (*Pinus contorta*) is the dominant tree species; Subalpine Fir (*Abies lasiocarpa*), Engelmann Spruce (*Picea engelmannii*), and Whitebark Pine (*Pinus albicaulis*) are also common. Forest composition at

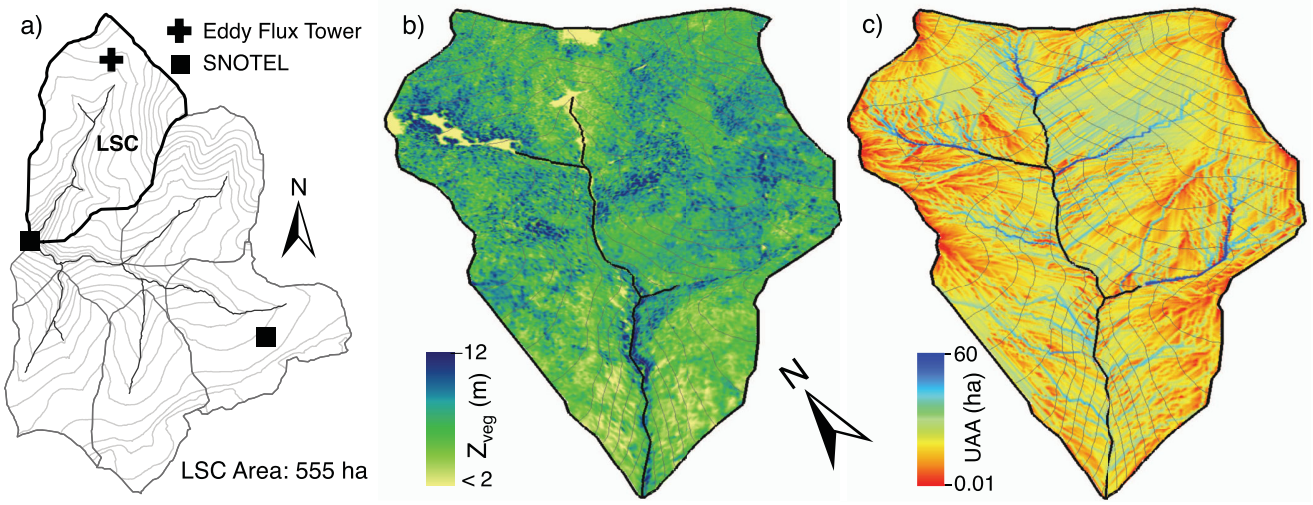

Figure 1. (a) Lower Stringer Creek (LSC) subwatershed within the greater Tenderfoot Creek Experimental Forest and locations of SNOTEL stations and eddy covariance tower. (b) Vegetation heights (10 m grid resolution) averaged from 1 m resolution LIDAR data. (c) Upslope accumulated area (UAA, 10 m grid resolution, logged color scale) calculated using a two-direction flow algorithm.

TCEF is a mosaic of different aged patches while most substantially large stands are single aged. The majority of LSC areas around the stream and north of the stream regenerated after two fires in the middle of the eighteenth century. The lower elevations experienced a stand-replacing fire in 1902. Especially stands in the southwestern portion of LSC were more affected by smaller, nonstand-replacing fires [*Barrett*, 1993]. The maximum tree height is just over 30 m. Shrubs and grasses are predominant in the riparian areas.

Soils at TCEF are loamy Typic Cryochrepts along hillslope positions and clayey Aquic Cryoboralfs in riparian zones and parks [*Holdorf*, 1981]. Based on the installation of >180 shallow groundwater wells, *Jencso et al*. [2009] found an average soil depth of about 1 m, ranging from 0.5 to 2 m.

The geology at TCEF consists of four different strata, all of which are present in LSC. Flathead Sandstone is the most dominant geologic layer in the midaltitude parts while the higher elevations are underlain by shale (Wolsey Formation) and biotite hornblende quartz monzonite. Granite gneiss occurs in the lower part of LSC [*Reynolds and Brandt*, 2006].

Climate at TCEF can be classified as continental. The average precipitation over the 1961–1990 base period was 880 mm [*Farnes et al*., 1995]. Approximately, 70% of the precipitation falls as snow. The main snowmelt period usually occurs between mid-May and the end of June, runoff normally peaks with snowmelt.

2.2. Hydrologic Measurements

Discharge for the study period (WY 2007–2008) was measured every 30 min with a 3.5 foot H-Flume at the LSC outlet using capacitance rods with ±1 mm resolution (TruTrack Inc., Christchurch, New Zealand) and later aggregated to an hourly time series. Precipitation and snowmelt were measured at two Natural Resources Conservation Service (NRCS) SNOTEL sites located within TCEF, one near the headwaters at 2259 m, and the other in proximity to the LSC outlet near the bottom of the Experimental Forest (1996 m) (Figure 1a). SNOTEL sites comprise a network of stations across the mountain west and Alaska recording precipitation, snow height, and snow water equivalent (the amount of water in a snowpack at a given time). Actual evapotranspiration (ET) was measured at an eddy-covariance tower located in the watershed (see Figure 1) and later aggregated to 60 min totals.

We used a separate snowmelt module that was not connected to the WECOH rainfall-runoff routine to generate spatially distributed precipitation and snowmelt from observations from two NRCS SNOTEL sites located at TCEF. The snowmelt model was effectively an interpolation tool and was calibrated outside of the WECOH runoff model structure for each year individually and its spatial snowmelt output became an external forcing to the core runoff model. Distributed watershed models that have a snowmelt routine

integrated into their greater model structure can be at risk of cocalibrating snowmelt and runoff, i.e., the modeled input may inadvertently be optimized to improve fits to observed runoff data. In our application, the decoupled snowmelt and rainfall-runoff routines are advantageous because it avoids potential cocalibration issues, resulting in an independent model input. We simulated distributed snow accumulation and melt, and liquid precipitation for each grid cell across the Stringer Creek watershed using an extended temperature index based model that allowed for cold content approximation following a method outlined by *Schaefli and Huss* [2011]. Details on the method and the calibration of the snowmelt model parameters can be found in Appendix A.

2.3. Disaggregation of Eddy Flux Measurements

The evapotranspiration point measurement from the eddy flux tower was disaggregated across the watershed on an hourly time step based on a linear relationship between height and leaf area index as suggested for these coniferous forests [*Keane et al*., 2005], similar to the derived distribution approach of *Emanuel et al*. [2011]. The eddy flux tower footprint has been estimated to cover the majority of the LSC subwatershed [*Emanuel et al*., 2010; *Mitchell et al*., 2015]. Treeless parks and meadows comprise less than 2% of the area in LSC and were assigned a 10% baseline of the tower measured ET for each time step. For much of the year, shallow soil moisture content at TCEF is <8–15%. By mid to late July the grasses have usually senesced, largely removing the transpiration component of ET with little shallow soil moisture for E. During and immediately following the short melt period, 10% baseline ET could be an underestimation, however we did not have data to further constrain it and chose simplicity rather than a time varying component.

Using the eddy-covariance point measurement, ET was disaggregated across the landscape with the following relationship:

$$ET_{mat} = base + ET_{flux} \times \left(zveg^{b_{et}} \times \left(\frac{ET_{flux} \times n - base \times n}{\sum_{i=1}^{n} zveg(i)^{b_{et}}} \right) \right) \quad (1)$$

where ET_{mat} is the resulting disaggregated *ET* matrix, ET_{flux} is the eddy-covariance point measurement, *base* is the base value of *ET* for each grid cell, *zveg* is the vegetation height matrix, b_{et} is the scaling factor, which was set to 1 for a linear relationship, and *n* is the number of watershed matrix cells. The approach is mass conserving, i.e., the mean ET of all cells equals the tower measurement. Similar to the decoupled snowmelt routine, treating ET as an independent external forcing rather than part of the rainfall-runoff calibration reduced the risk of cocalibration between ET and runoff.

The vegetation height was calculated by subtracting the ground returns (bare earth) from the first returns (elevation of canopy) of the 1 m LIDAR coverage. The resulting vegetation heights were subsequently resampled from a 1 m grid resolution to 10 m by averaging the 1 m vegetation heights. A 10 m DEM resolution was found to provide the most realistic representation of the local topography for representing subsurface flow without being overly influenced by surface microtopography, e.g., rocks or fallen logs. Past work at the site has also shown that representation at this resolution was most consistent with observed shallow water table dynamics [*Jencso et al*., 2009].

2.4. Watershed Ecohydrology Model (WECOH)

WECOH is a parsimonious but fully spatially distributed rainfall-runoff model that explicitly incorporates topographically driven lateral water redistribution and water uptake by vegetation. The only inputs to the model are a digital elevation model (DEM), gridded vegetation height, a precipitation/snowmelt time series, and evapotranspiration from an eddy flux tower (or independently modeled or estimated ET). For computational reasons, we ran the model on a 60 min time step, but shorter time steps are possible. The model requires only four parameters, two of which were fixed (Table 1). WECOH calculates a water balance for each 10 m grid cell:

$$\frac{dS}{dt} = P + I - O - ET \quad (2)$$

where *dS*/*dt* is the change in cell storage (mm) over the time step *t*, *P* is incoming precipitation or melt (mm) derived from the snowmelt model, *I* is inflow from other cells (mm), *O* is outflow out of the cell (mm), and *ET* is evapotranspiration (mm). Water is routed downhill on a grid cell to grid cell basis using a flow

Table 1. WECOH Model Parameters

Parameter	Description
$Cond_{max}$	Maximum conductivity
b	Shape parameter for the storage-release function
S_{max} (fixed)	Maximum storage capacity
Vel_{stream} (fixed)	Stream velocity

algorithm similar to *Quinn et al.* [1991] that proportionally routes water down the two steepest gradients. Conductivity is calculated with a simple storage-release function:

$$Cond = Cond_{max} \times \left(\frac{S}{S_{max}}\right)^{b} \quad (3)$$

where $Cond$ is conductivity (mm/min), $Cond_{max}$ is the maximum conductivity (mm/min), S is actual cell storage (mm), S_{max} is the maximum possible storage (or effective storage, mm), and b is the shape parameter of the storage-release power function that determines the degree of concavity (Figure 2) of the storage-conductivity relationship. Cell outflow is then calculated using the cell cross-sectional area (assuming a uniform soil depth of 1 m) and the gradient between two cells (approximated by local topography):

$$O = \frac{Cond \times A_{cross} \times grad \times t}{A_{cell}} \quad (4)$$

where O is cell outflow in m, $Cond$ is conductivity (m/min), A_{cross} the cell cross-sectional area (m^2), A_{cell} is the grid cell area (m^2), $grad$ the dimensionless gradient to the downslope cell, and t is the time step (min).

The model formulation in WECOH updates storage in an explicit manner, which *Kavetski and Clark* [2011] demonstrated can lead to a sawtooth pattern in cell outflows. To prevent this, cell storage was reevaluated every 10 min during the 60 min time step to adjust actual storage and cell outflows.

We did not evaluate model performance with different grid sizes, but acknowledge that the model parameters could be dependent on grid resolution, likely similar to other commonly applied hydrologic models. Here for consistency with prior research conducted at TCEF—including the empirical analysis of *Jencso et al.* [2009]—we selected the 10 m resolution.

Cells less than 3 m in elevation above the stream cells were designated riparian cells, comparable to *Jencso et al.* [2009, 2010], and their gradient was fixed at 0.01 to account for only partial stream penetration of riparian soil profiles and low-gradient valley bottoms relative to adjacent uplands. Similar to DHSVM [*Wigmosta et al.*, 1994], the model does not have an infiltration routine and all precipitation immediately becomes storage if the cell is not saturated and can accommodate the incoming precipitation amount. Excess water, the ponded water of oversaturated cells, is routed downhill along a flow path to the next unsaturated cell, until all overland flow has either become cell storage or reached the stream. Once the water from the hillslopes reaches the stream, it is routed downstream with a constant velocity, Vel_{Stream}.

2.5. Model Calibration and Parameter Values

Runoff and ET data were available for three consecutive years, 2006, 2007, and 2008. Precipitation data were available for 2007 and 2008. Since only incomplete precipitation data were available for 2006, we duplicated the 2007 WY and used it as warm-up for the 2 year model simulation period 2007–2008. We used the model as a diagnostic—rather than a forecasting—tool to inform on runoff source areas during the 2007–2008 study period. For this reason, we calibrated the model on the study period data and refrained from a validation period, which is common for models primarily used for forecasting. Calibrations were performed on averaged daily runoff values to integrate pronounced daily melt and refreeze dynamics.

S_{max} was fixed at 500 mm to approximate actual soil properties at TCEF, Vel_{stream} was set to 10 m/min but model performance was found to be insensitive to variations in the parameter in early model simulations, likely because of the overall short stream length in LSC (2.9 km for main channel). The two remaining parameters, $Cond_{max}$ and b, were calibrated with 5000 Monte Carlo simulations using the observed hydrographs for the 2007 and 2008 WYs. We calculated Nash-Sutcliffe efficiencies (NSE) for both years separately as well as over the full 2 year calibration period.

2.6. Active and Contributing Watershed Area

We determined a storage threshold on the storage-release curve below which a cell was considered inactive for our analysis of active and contributing watershed areas. An active cell transmits water to the cells immediately downslope. However, even inactive cells can transmit water downslope, but because of low

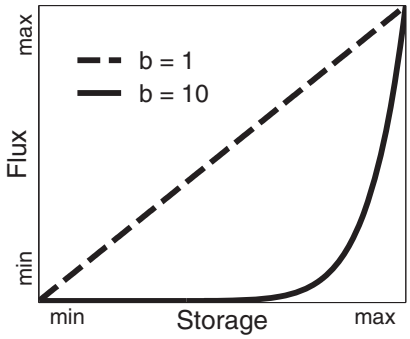

Figure 2. Relationship between cell storage and resulting flux. Pictured are two hypothetical relationships for different values of the shape parameter *b* (equation (2)). $b < 1$ is not shown as it would result in an unrealistic storage-flux relationship.

transmissivities below a certain storage threshold, those amounts are insignificant when compared to the amounts transmitted by the wetter, active cells. A "contributing cell" is an "active cell" whose downslope flow paths are entirely active and end in the stream [*Ambroise*, 2004]. Active cells may become disconnected from the stream network, forming insular patches of active, but noncontributing cells when sections of flow paths become inactive. The contributing watershed area at any point in time is therefore always equal to or smaller than the active watershed area.

The storage threshold for active and inactive cells was determined based on an empirical connectivity duration curve established for TCEF by *Jencso et al*. [2009]. Based on water table observations from 84 recording shallow groundwater wells, *Jencso et al*. [2009] quantified a linear relationship between the size of the upslope accumulated area (UAA) of a hillslope and the duration a water table existed (binary observation, water table present or not) above the bedrock interface across the hillslope-riparian area-stream continuum for the 2007 water year. They extrapolated the relationship to all hillslope cells bordering the riparian area. This resulted in a saturated throughflow connectivity duration curve (CDC) that informs how much of the hillslope network was hydrologically connected to the stream network. This concept has since been successfully applied at TCEF with the semidistributed Catchment Connectivity Model (CCM) framework [*Smith et al*., 2013]. Here we used the empirical network connectivity duration curve to calibrate a watershed-scale threshold for active/inactive cells. We calculated network connectivity, i.e., the number of hillslope cells bordering the riparian zones that were connected to the stream network, for 1–500 mm thresholds in 1 mm increments on a daily basis for the 2007 water year, resulting in 500 modeled network connectivity curves (see section 3 for details). For example, there are 594 lower hillslope cells that are adjacent to the riparian area. If 60 cells exceeded a given storage threshold, it would result in a network connectivity of 10.1%. The modeled network CDCs were compared to the empirical network CDC from *Jencso et al*. [2009] using Nash-Sutcliffe efficiencies. The grid size used to derive both the empirical as well as modeled CDCs was 10 m. The storage threshold that resulted in the best fit to the empirical CDC was used as the threshold to determine active from inactive cells in WECOH.

We calculated active and contributing areas for every hour of the simulation period but here present 12 characteristic days (6 days in each year) that cover the range of runoff conditions. It is important to note that the active and contributing areas differ from the network connectivity. Network connectivity only applies to the lower hillslope cells, while active and contributing areas refer to the entire watershed area (all cells within the watershed). For each of the 12 days, we calculated the hillslope width functions, W(x), of the contributing area. A hillslope width function is essentially a frequency distribution of flow path lengths for hillslope cells to a stream cell along a flow path [e.g., *Troch et al*., 1994; *D'Odorico and Rigon*, 2003; *Bogaart and Troch*, 2006]. The cell count is then rescaled by the total amount of hillslope cells (55,240). In the case of the entire DEM, the area under the width function is equal to 1; for the contributing portions of the watershed, the area under the curve equals the fraction that is contributing area.

3. Results

3.1. Snowmelt and ET

Annual *P* in both 2007 (916 mm) and 2008 (874 mm) was close to the average of the 1961–1990 base period of 880 mm. The snowmelt model calibration resulted in good fits for the 2007 and 2008 water years, with NSEs between observed and simulated SWE time series ranging from 0.85 to 0.99 (see Table A1 in Appendix A for the calibrated parameters and efficiencies, Figure A1 for simulated and observed SWE time series, and Figure A2 for distributed maximum SWE and timing of meltout). In 2007, 668 mm of *P* fell in the form of snow (73% of total annual *P*) and in 2008 snowfall was 735 mm and comprised 84% of annual *P*. At

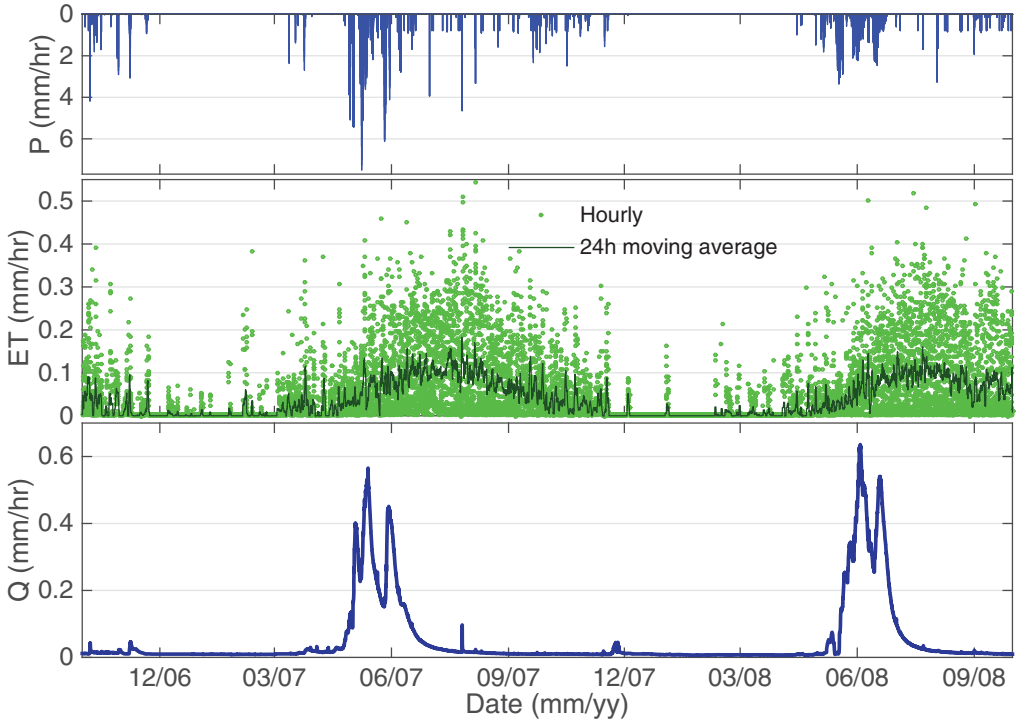

Figure 3. Overview of precipitation (*P*), evapotranspiration (ET), and runoff (*Q*) data for the simulation period.

the time of greatest SWE accumulation, minimum simulated SWE (lowest elevation) in 2007 and 2008 were 260 mm and 313 mm, respectively, while maximum simulated SWE (highest elevation) in 2007 and 2008 were 533 and 592 mm, respectively.

The hourly evapotranspiration measured at the eddy-covariance tower was variable, as is typical of fine time scale latent heat fluxes (Figure 3, middle). Annual ET was 483 mm for 2007 and 449 mm for 2008. Sublimation from the snowpack and canopy can constitute an important part of the annual snow energy balance [e.g., *Dozier and Melack*, 1987; *Molotch et al*., 2007]. Without adjustment, sublimation water fluxes can artificially increase the tower-based estimate of ET. Here we approximated sublimation from the snowpack with the eddy covariance-derived latent heat flux time series. For the adjustment, we assumed that, when a snowpack was present, latent heat flux measured at the eddy-covariance tower at temperatures below 0°C was sublimation from the snowpack rather than transpiration. Therefore, our estimates of ET and hence extraction from soil and shallow groundwater were not influenced by sublimation of snow.

Annual sublimation losses from the snowpack were 105 mm in 2007 (11% of *P*) and 126 mm in 2008 (14% of *P*). This reduced melt water input to the ground to 556 mm in 2007 and 596 mm in 2008. These sublimation losses are comparable to sublimation values reported by *Hood et al*. [1999] for Niwot Ridge (195 mm, or 15% of the max snow accumulation). The adjusted annual ET totals (water that will be removed from the soil column during the model simulation) were 378 mm in 2007 and 323 mm in 2008.

3.2. Runoff Calibration

The highest Nash-Sutcliffe efficiencies for calibration on the individual water years were 0.8 for 2007 and 0.94 for 2008 (Figure 4, left and middle). The highest NSE over the entire 2 year simulation period was intermediate with 0.86 (Figure 4, right). However, high Nash-Sutcliffe efficiencies were achieved over a range of parameter combinations, especially in 2008, where efficiencies greater than 0.9 were reached over much of the parameter space (see inner contour line in Figure 4, middle). Multiple parameter combinations resulted in NSEs that were similar to the third decimal place. We averaged the parameters of the 20 best runs for the combined calibration (all identical efficiencies) to obtain an optimal parameter set. The averaging resulted in a parameter combination that matched the highest efficiency on the combined parameter-efficiency

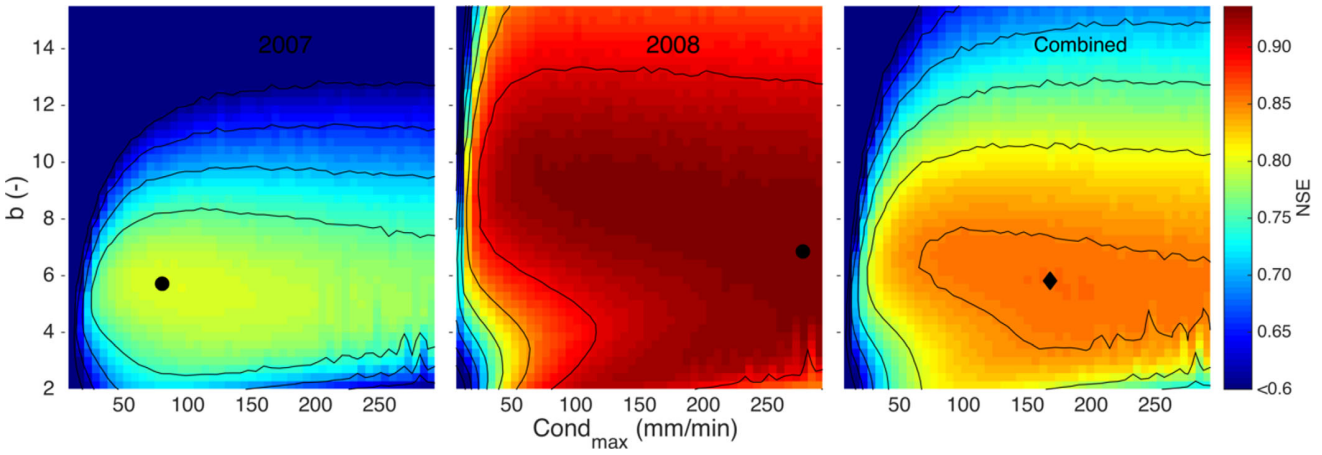

Figure 4. Parameter surfaces for runoff calibration for the (left) 2007 and (middle) 2008 WYs, and (right) the combined calibration for both years. It is important to note that the "combined" surface was not derived by averaging the "2007" and "2008" surfaces, but shows the NSE surface for 2 year runs. The optimal parameter combinations for 2007 and 2008 are denoted by the black dots, the final parameter combination is denoted by a black diamond.

surface grid. However, similar efficiencies were derived for $Cond_{max}$ and b parameters within 15% and 20%, respectively, of the optimum value. The optimal parameter set for the 2 year period calibration resulted in $Cond_{max}$ and b parameter values of 167 mm/min and 5.82, respectively. While the simulated runoff hydrograph matched the observed runoff well, especially in timing, it generally overestimated peak runoff in 2007 and underestimated peak flows in 2008 (Figure 5). The final recession periods were slightly overestimated in 2007 but matched the observed falling limb of the hydrograph well in 2008.

3.3. Calibration of Storage Threshold

The empirical connectivity duration curve developed by *Jencso et al.* [2009] (Figure 6, black lines in main figure and inset) indicates a maximum connectivity of the stream network to the hillslopes of 72%. Connectivity quickly decreased to approximately 10% at 20% exceedance (i.e., 20% of the time are 10% or more of the network connected). For 50% of the year, the connectivity is below 5%. Calculating the simulated connectivity duration curves for all possible thresholds between 1 mm (i.e., always connected) and 500 mm (only connected at full saturation) resulted in an ensemble of CDCs (Figure 6, inset). The calibration of the connectivity duration curves (CDC) to distinguish between active and inactive cells resulted in a maximum NSE of 0.98 at a storage threshold of 293 mm (Figure 6, red line in main figure). However, NSEs were nearly identical over a range of $\pm$4 mm around the 293 mm storage threshold, only differing in the third decimal. The calibrated peak network connectivity for 2007 slightly overestimated (at 81% versus 72%) the empirical CDC. The largest differences in the CDCs occur between approximately 15% and 30% annual exceedance, when the simulated CDC slightly underestimated network connectivity. However, a linear regression between the observed and simulated CDCs reveals a good fit, with the regression line matching the 1:1 line closely (Figure 7). The 293 mm activation threshold resulted in a conductivity value of 7.5 mm/min on the calibrated storage-release curve (Figure 8). Conductivities were generally very low ($<$2 mm/min) below 200 mm of storage.

3.4. Evolution of Watershed Connectivity

The extent of active area was smallest during the base flow period from summer through spring, before snowmelt started (Figures 9a and 9f for 2007 and Figures 9g and 9l for 2008 and Table 2), with less than 2% of the watershed active (by the definition set forth is this paper). With the onset of snowmelt in the lower elevations, areas in the lower part of the watershed became active (Figure 9b). Over the course of the melt period in 2007, the mid and upper sections of the watershed became active (Figures 9c and 9d) until toward the end of snowmelt, runoff was mostly generated in the higher elevations and larger drainages in the lower elevations (Figure 9e). During peak flow approximately 76% of the watershed area was active. Less than 2.5 months after peak runoff, only 2% of the watershed areas were active and only the largest drainages contributed to stream runoff (Figure 9f). During the 2008 melt period, the onset of melt was more

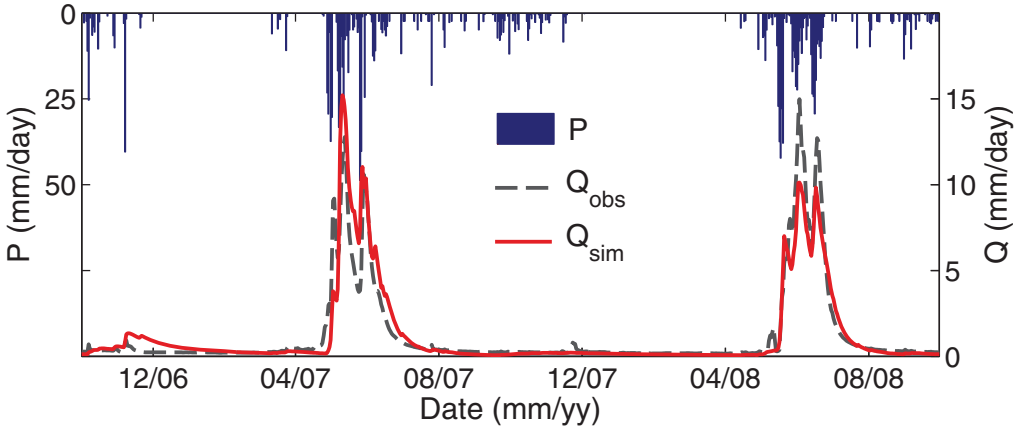

Figure 5. Average simulated precipitation (rain and snowmelt) and observed and simulated runoff for the 2 year simulation period.

homogenous with approximately equal areas in upper and lower elevations being active (Figures 9h and 9i). Active areas during the later part of melt were focused on the midsections and upper sections similar to 2007 (Figures 9j and 9k).

Contributing areas were highly spatially and temporally variable within years but showed similar patterns in both years of the study period (Figure 10, blue-shaded areas). A Pearson correlation coefficient between upslope contributing area and the fraction of time a hillslope cell was connected to the stream network was $r_p = 0.69$. For purely topographically controlled water redistribution, this correlation could be expected to be closer to 1. However, water uptake by vegetation is an important factor that exerts a control on the storage in a cell and both upslope and downslope flow path connectivity and water redistribution. Spatially disaggregated ET leads to heterogeneous water withdrawal, further decreasing the correlation between UAA and storage. Other confounding factors influencing storage—and thus connected area—include spatially variable snow accumulation and melt/precipitation dynamics. There was a considerable difference in snow

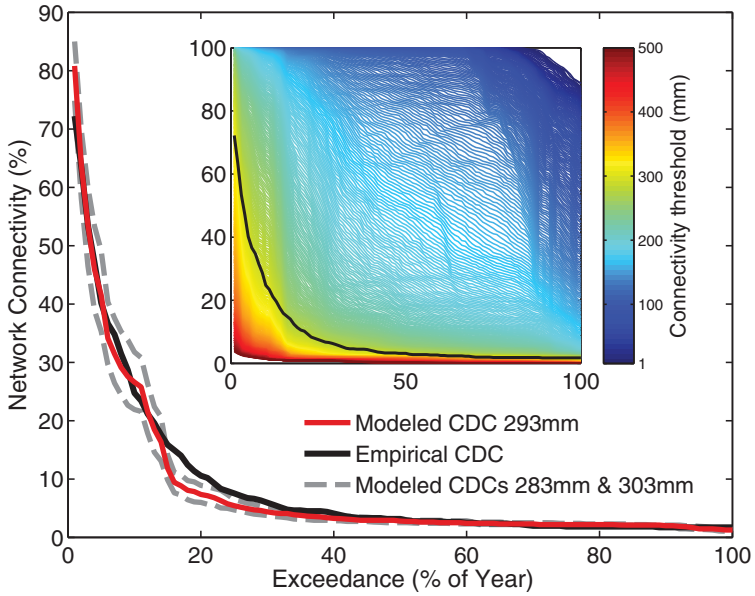

Figure 6. Empirical connectivity duration curve [*Jencso et al.*, 2009], denoted by black line, and modeled connectivity duration curve for hillslope-riparian-stream connectivity. A storage threshold between active and inactive cells of 293 mm resulted in a CDC that best fit the empirical CDC (denoted by the red line). Two CDCs 10 mm below and above the best threshold are shown for comparison (denoted by gray dashed lines). The inset shows the suite of CDCs from 1 to 500 mm thresholds in 1 mm increments as well as the empirical CDC.

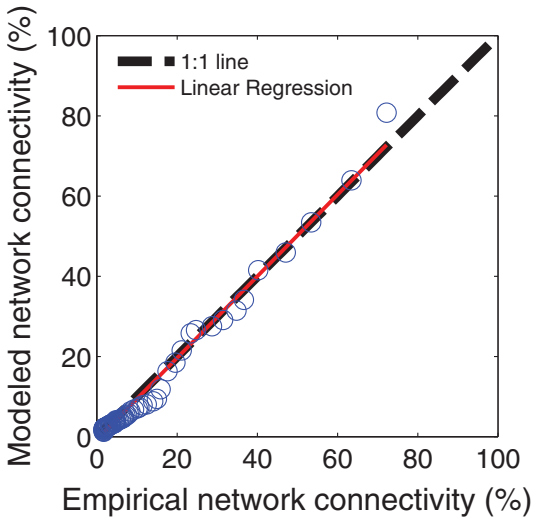

Figure 7. Bivariate plot of empirical and modeled CDC (blue circles) as well as the 1:1 line between them and the result from a simple linear regression between the two curves.

accumulation between the lower and higher elevations in both 2007 and 2008, with the highest elevation DEM cell accumulating 273 and 279 mm, respectively, more SWE than the lowest elevation DEM cell. Exceeding the storage threshold for connectivity for cells with similar upslope area is thus more likely for higher elevations that received more snow. The resulting spatial patterns of the active and contributing areas were thus a result of topographically driven lateral water redistribution, water uptake by vegetation, and spatially variable precipitation and snowmelt inputs.

The active and contributing areas at equal runoff were very different for the rising and the falling limb of the snowmelt generated hydrographs in both years (Figures 10 and 11). Some of these differences include the low elevation active areas that were more prominent on the rising limb with high elevations producing more of the runoff on the falling limb, contributing to hysteretic behavior in runoff source areas (Figure 11, left). The differences in 2008 were less pronounced overall. In 2008, the higher elevations were the dominant source of runoff at the selected discharge levels on both the rising and falling limb of the hydrograph (Figure 11, right).

The differences in runoff source areas become more apparent in the hillslope width functions (Figure 12). The contributing area width functions indicate how far away from the stream network the contributing areas are (following their downslope flow paths). In both years, approximately 35% of premelt runoff was generated mainly in near-stream and riparian areas at a distance of less than 60 m from the stream (black solid lines in Figure 12). With beginning snowmelt, those areas expanded to more locations parallel—and close—to the stream network. During the initial rising limb of the hydrograph in 2007, 56% of runoff was generated on areas less than 300 m from the stream network (Figure 12, 8 May in top plot). Subsequently hillslopes became active and during peak flow. In addition to the initially stream-parallel expansion of contributing areas, when riparian and near-stream areas started contributing, hillslopes along the stream began to contribute to runoff. At peak flow, 50% of contributing areas were at distances of less than 450 m and 500 m in 2007 and 2008, respectively (Figure 12, 10 May in top plot and 3 June in bottom plot). A shift occurred during the later stages of the snowmelt event, when more areas at distances >500 m became connected, while simultaneously small hillslopes became disconnected. As a result, during the final streamflow recession in both 2007 and 2008, 59% and 67% of runoff, respectively, were generated on areas at distances of at least 500 m from the stream network (Figure 12, 3 June in top plot, 27 June in bottom plot).

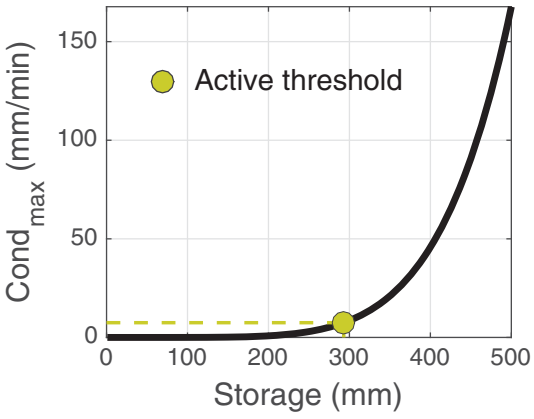

Figure 8. Storage-release curve with calibrated model parameters as well as the threshold for active/inactive cells at 293 mm (denoted by the yellow circle).

Even though the maximum area connected at any day in the 2 year study period was 71%, over the course of the 2 years 90% of the cells became active for at least 1 day (Figure 13). The areas that never connected to the stream network were only 10% of the watershed. Those dry areas were located on the (mostly) subtle ridges between the larger hillslope drainages but there were also small individual patches that receive only few inflows, nested within the large drainage networks (Figure 13). The average active and contributing

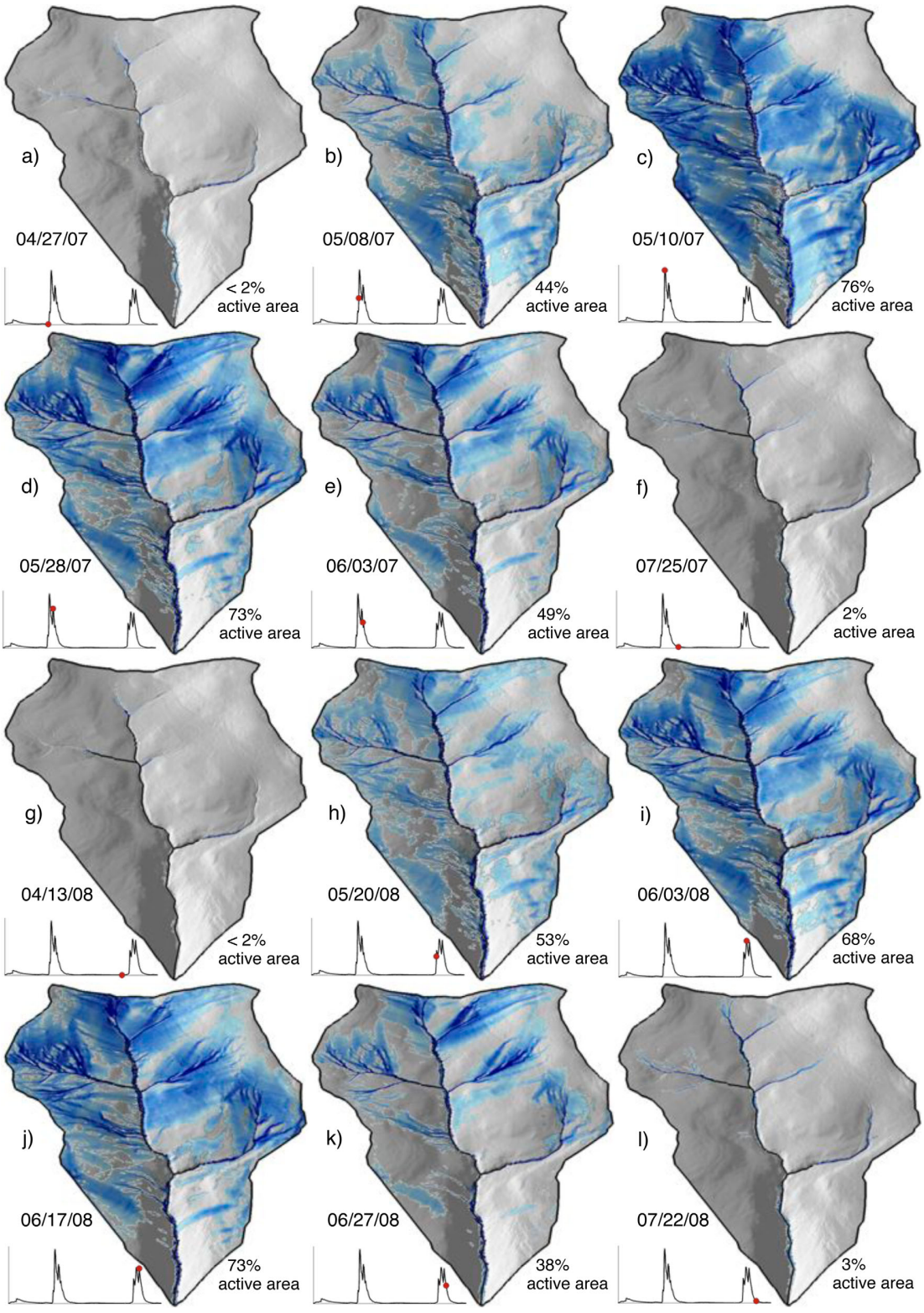

Figure 9. Evolution of watershed active area over the course of the 2007–2008 study period. Gray areas were below the 293 mm storage threshold and thus inactive. The blue shading denotes the degree of storage, with light blue areas at 293 mm to dark blue areas at 500 mm. The insets show the time of the snapshot on the hydrograph for reference.

Table 2. Active, Contributing, and Active Noncontributing Area, as Well as Runoff for 12 Characteristic Days of the 2 Year Study Period

Date	Active Area (%)	Contributing Area (%)	Active, Disconnected Area (%)	*Q* (mm/d)
27 Apr 2007	<2	<2	0	0.16
8 May 2007	44	28	16	7.26
10 May 2007	76	71	5	14.52
28 May 2007	73	57	17	11.04
3 Jun 2007	49	35	14	7.20
25 Jul 2007	2	<2	<1	0.30
13 Apr 2008	1	1	0	0.06
20 May 2008	53	27	26	5.26
3 Jun 2008	68	52	16	10.13
17 Jun 2008	73	57	15	9.83
27 Jun 2008	38	26	12	5.08
22 Jul 2008	3	2	1	0.60

areas over the 2 year simulation (731 day) period were 7.9% and 5.7%, respectively.

4. Discussion

Despite long-term effort by the hydrologic community, tracing streamflow back to its source areas remains a challenge. To partially address this, we developed and present a parsimonious rainfall-runoff modeling framework that allows for tracking of the spatial distribution of watershed storage and thereby watershed runoff source areas. Utilizing empirical measurements of hillslope-riparian-stream connectivity, we approximated active and contributing areas based on a calibrated storage threshold. The discussion focuses on general model performance, the meaningfulness of the calibrated storage threshold, and the implications of temporally variable contributing areas for predicting and interpreting observed streamflow dynamics.

4.1. Model Assessment

4.1.1. Calibration

The runoff simulated over the 2 year period matched the observed runoff well with a NSE of 0.86 over the two simulated water years. While fitting the hydrograph is the minimum requirement for any hydrologic model, we were particularly interested in the spatial distribution of storage in order to use the model as an interpretative tool to learn about watershed functioning. The resulting storage patterns for both years reflected a realistic scenario with carry-over storage magnitude and patterns from 1 year to the next. Single-year calibration storage states optimized for individual years could either retain or release too much water in the alternate year, thereby matching an individual year's hydrograph well at the expense of the alternate year(s). This suggests and reinforces the importance of antecedent conditions and model conditioning. In fact, numerous studies have documented the strong memory effect of watershed storage state on future runoff behavior [e.g., *Fedora and Beschta*, 1989; *Binley and Beven*, 1992; *Istanbulluoglu et al*., 2012].

4.1.2. Internal Functioning and Structure

Despite the reasonable fit to the hydrograph, the question remains whether the simplified model structure adequately captures the runoff processes at TCEF. The timing and peaks of the simulated runoff time series match the observed runoff well during the melt period and, like the observed runoff, the model does not respond to summer storms. Summer precipitation events at TCEF usually do not lead to an increase in streamflow. The precipitation gets absorbed in the upper centimeters of the soil and subsequently evaporates, similar to what *McNamara et al*. [2005] reported from a watershed in Idaho with comparable climatic conditions.

Runoff source areas exhibited a strong topographic control during snowmelt and extended far up the hillslopes, with smaller hillslopes becoming connected during the main melt period. During the recession period, the contributing areas contracted and only left main drainages and channel heads active. This is on accordance with empirical observations at TCEF that determined that topography drives hydrologic response during the melt period [e.g., *Jencso et al*., 2009; *Jencso and McGlynn*, 2011; *Payn et al*., 2012]. The good fit between the simulated and empirical connectivity duration curves furthermore exemplifies this.

However, while the general runoff dynamics were captured well, the model overestimated runoff in the fall of 2006 and slightly underestimated the initial rising limb of the 2007 melt period. However, it is important to note that those under and overestimations are likely exacerbated by the modeled precipitation input. While the modeled input is reasonable, it simulates a brief but intense melt period at the Stringer Creek SNOTEL site in early October 2006 with 60 mm of melt over the course of 10 days. This melt period does

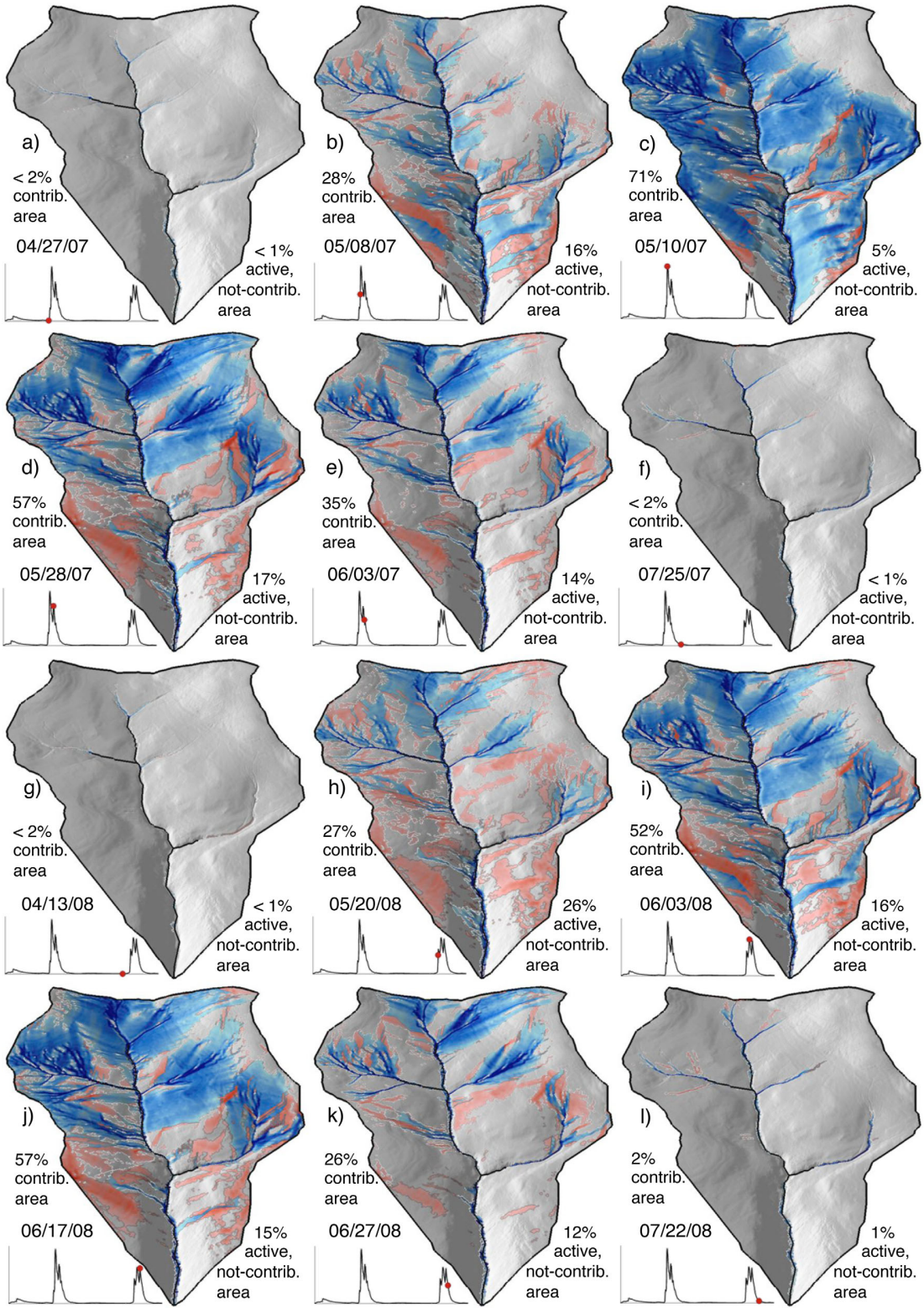

Figure 10. Extent of active and contributing areas at nine spatial snapshots in time. Blue color denotes contributing areas; active, noncontributing areas are shown in red. The shading denotes the degree of storage, with light blue/red areas at 293 mm to dark blue/red areas at 500 mm. The insets show the time of the snapshot on the hydrograph for reference.

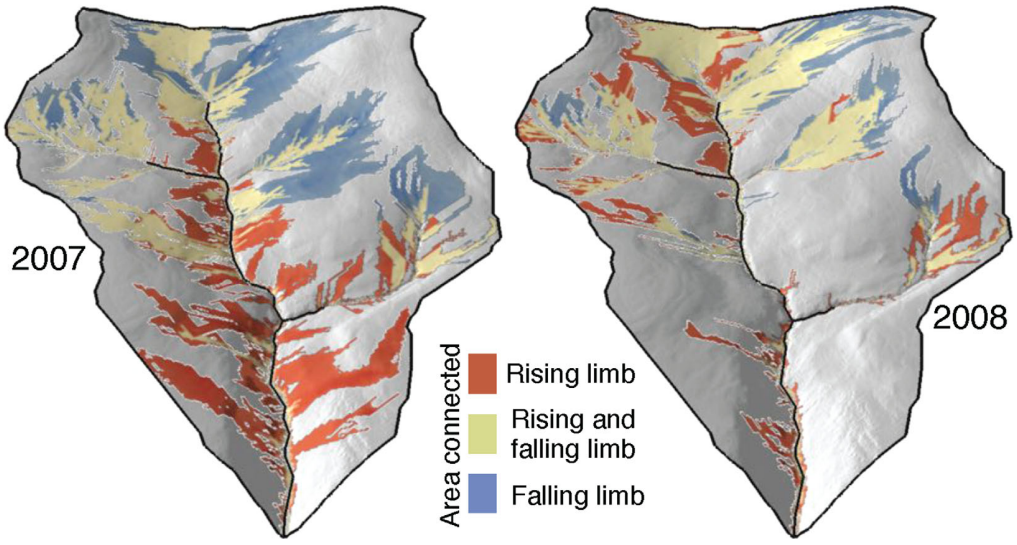

Figure 11. Connected areas on a day on each the rising and falling limb for the 2007 (8 May and 3 June) and 2008 (20 May and 27 June) water years. Runoff on select days on the rising and falling limb of each year was approximately equal.

not occur in the observed melt record at the site. Likewise, the delayed response in simulated runoff is probably caused by a delayed melt input, i.e., the observed runoff begins to increase 2–3 days prior to the onset of simulated melt. Regardless, these details do not impact the general model behavior but rather indicate model and system sensitivity to precipitation.

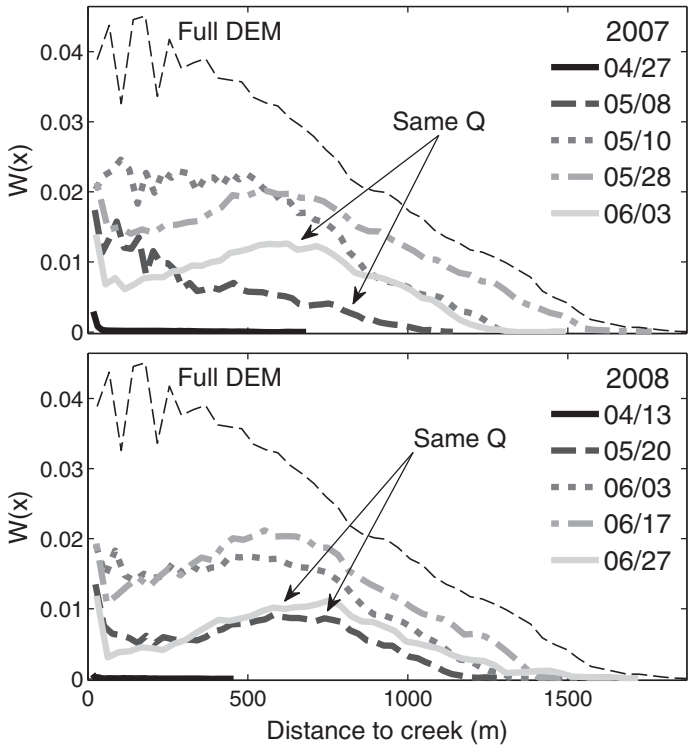

Figure 12. Hillslope width functions for contributing area at 5 days from the (top) 2007 and (bottom) 2008 water years. The thin dashed line shows the hillslope width function for the entire watershed for reference.

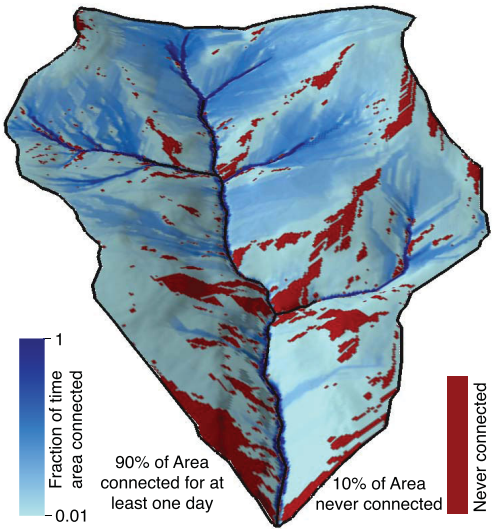

Figure 13. Connected areas (shades of blue) and areas that never connects (red) over the course of the 2 year study period. Color scale is logged for better visualization.

In addition to uncertainties in the simulated input, the underestimation of runoff peaks in 2008 may hint that the watershed potentially became too dry over the 8 months base flow period during the simulation. As a consequence, cell storage states during peak melt may not increase sufficiently to achieve high flux rates. Owing to the nature of the highly nonlinear response function, even small differences at high storage states will lead to larger changes in the resulting flux than the same difference at smaller storage states (Figure 8), for example, the increase in *Cond* from 300 mm storage to 320 mm is 3.9 mm/min, while the increase from 450 mm of storage to 470 mm is 26.2 mm/min.

A possible explanation for overly dry watershed conditions could be the lack of a deeper groundwater component in WECOH as all runoff is generated in the soil horizon from the watershed uplands. While this is a justified assumption for the melt period, this may not be true for the base flow period. It has previously been documented that hillslope soil water alone can sustain base flow [*Hewlett and Hibbert*, 1963], but there is evidence at TCEF that at least during base flow some of the runoff may originate from deeper groundwater layers. *Jencso and McGlynn* [2011] and *Nippgen et al*. [2011] determined that elevated base flow levels and delayed response times were evident in subwatersheds at TCEF underlain by sandstone as opposed to subwatersheds without sandstone surficial geology. This suggests increased recharge into the bedrock groundwater during the melt season and subsequent extended outflow during the growing season, thereby sustaining more elevated base flow in some of the TCEF subwatersheds. *Jencso and McGlynn* [2011] documented and *Payn et al*. [2012] further suggested that the hydrologic controls on runoff at TCEF may shift from mainly topography-dominated flow during the snowmelt period to increasing groundwater contributions toward the end of the growing season and through the winter.

Not including groundwater flow in WECOH may lead to artificially high simulated drainage of the watershed uplands and thus to storage conditions at the end of the base flow period that are too low to (a) be responsive enough at the beginning of the melt period, or (b) raise storage at peak flow to storage states that allow for greater water flux. If the cells around the stream within WECOH dry down too much over the course of the summer and through the winter, the initial melt magnitudes may not suffice to raise cell storage enough to achieve higher conductivities for an increase in streamflow. However, it is uncertain if the underestimation of peak runoff in 2008 is a result of storage states that are too low or if it is related to the spatiotemporal estimation of melt and precipitation inputs. Although including a deeper groundwater component in WECOH might slightly improve the response in the early stages of snowmelt or at peak flow, WECOH's simple model structure appears to adequately represent the hydrologic behavior of the study period.

4.1.3. From Storage to Contributing Areas

Our objective was to develop and evaluate a parsimonious distributed water balance model to inform understanding of streamflow source areas through time. In order to translate information on distributed storage state to dominant runoff source areas, we built on widely recognized threshold behavior in hydrologic systems. For example, at Maimai in New Zealand, *Mosley* [1979] documented that exceedance of a rainfall threshold led to activation of preferential flow pathways (i.e., macropores) and rapid water delivery to the stream network. *Woods and Rowe* [1996] further observed rainfall thresholds that led to variable hillslope trench face runoff magnitudes. *McGlynn and McDonnell* [2003a] later separated watershed response—also at Maimai—into contributions from riparian areas and hillslopes and concluded that hillslope areas delivered water in addition to the riparian areas as a function of precipitation magnitude and

initial soil moisture conditions. These behaviors are similar to what we observed in our study, where at first the runoff source areas were limited to near-stream riparian areas and then extended to the hillslopes as the distributed storage states increased. Precipitation thresholds above which saturated hillslope throughflow response increased were also determined in other geographic regions such as the Panola Mountain Research Watershed [*Tromp-van Meerveld and McDonnell*, 2006b]. However, in most cases, it is likely not just a simple precipitation threshold, but as *McGlynn and McDonnell* [2003a] suggest, a combination of precipitation magnitude and antecedent soil conditions that lead to saturated hillslope throughflow initiation. Therefore, here we did not approximate the connectivity threshold as a precipitation/melt depth but rather as storage state. Since surface runoff at TCEF is restricted to limited areas even during the wettest times, we focus on thresholds for subsurface flow initiation.

We used the connectivity duration relationship established by *Jencso et al*. [2009] to calibrate the threshold for active/inactive cells. This approach resulted in a storage threshold of 293 mm below which we consider a cell as inactive. Assuming a uniform soil depth of 1000 mm and 50% porosity, this translates to 29% volumetric soil water content (SWC) when integrated over the entire soil profile. This value is similar to SWC thresholds reported at other sites, e.g., 45% at 0–30 cm soil depth in a watershed in the Italian Alps [*Penna et al*., 2011] and 37% at 70 cm soil depth at the Panola Mountain Research Watershed [*Peters et al*., 2003]. At TCEF, *Jencso et al*. [2009] determined that hydrologic connectivity was tied to the establishment of a shallow water table on the bedrock-soil interface (saturated throughflow). In the WECOH model, calibration of the storage threshold to differentiate between active and inactive cells was based on *Jencso et al*.'s [2009] empirical water table observations (i.e., distillation of water table time series to a binary variable of presence/absence). The storage-conductivity relationship used in WECOH itself does not differentiate between saturated and unsaturated conditions. It is therefore a threshold above which the rate of water delivery down-gradient changes more abruptly.

Lehmann et al. [2007] argue that a mean threshold for flux initiation may not be an adequate assumption because of hillslope heterogeneity. For example, the fill-and-spill hypothesis for a hillslope throughflow, as outlined by *Tromp-van Meerveld and McDonnell* [2006a], suggests that flow on hillslopes initiates when depressions in the bedrock surface fill up and then water spills out of those depressions to fill up other depressions. The maximum outflow originates after all depressions have been filled. While conceptually compelling at the small scale in certain environments, the hillslope-specific details of fill-and-spill are likely not a widely significant factor at the watershed scale where hundreds of hillslopes of varying length and area contribute to streamflow. At the watershed scale, the details of individual hillslope fill-and-spill patterns (if they exist) would be subsumed into our threshold connectivity observations [*Jencso et al*., 2009]. An individual hillslope could differ slightly from the watershed-averaged threshold, however the strong relationships observed by *Jencso et al*. [2009] between upslope area and water table development suggests that the details of individual hillslope patterns are less critical for general behavior.

While a large distribution of hillslope sizes could average out some structural heterogeneity, it could also introduce issues in determining a response threshold based on precipitation. Although individual hillslope throughflow development has often been associated with precipitation thresholds [e.g., *Buttle et al*., 2004; *Tromp-van Meerveld and McDonnell*, 2006b; *McGuire and McDonnell*, 2010], it was likely often due to hillslope storage thresholds rather than event size per se. In this case, different size hillslopes would have different precipitation/input thresholds for hydrologic response because of the storage potential and legacy of past precipitation and redistribution downslope. This means larger hillslopes would require less precipitation to connect hydrologically via shallow throughflow to downslope riparian zones and streams because of their size [cf. *Jencso et al*., 2009]. In fact, this is a basic premise of the Catchment Connectivity Model (CCM) recently described by *Smith et al*. [2013] that has been shown to represent streamflow and be consistent with internal watershed observations of hydrologic connectivity (albeit at the semidistributed hillslope scale). There is some similarity to the manner in which stream channel initiation thresholds generally depend on contributing area but where streamflow initiation through time is also sensitive to storage/precipitation thresholds [e.g., *Montgomery and Dietrich*, 1992]. Thresholds based on storage/soil water content conditions encompass both area and precipitation, making them more robust to heterogeneities in watershed structure and hillslope size.

We acknowledge that in some watersheds connectivity could additionally result from the activation of preferential flow pathways. However, the storage-based subsurface throughflow threshold in WECOH provides

robust representation of general hydrologic response (streamflow, storage patterns) and therefore shows strong promise as a tool for inferring watershed-scale processes including the documentation of time varying contributing areas.

4.2. Variable Contributing Area

Variation in the spatial extent of contributing area ranged from less than 1% in the fall and winter to more than 70% during peak snowmelt (Figure 10). This represents an effective watershed area that changed from hour to hour, with effective watershed area defined as the area actively contributing to the runoff generation process at any point in time. This effective watershed area could be located near the stream network or in distal portions of the watershed. It follows then that a second assessment of an area's influence on watershed runoff would include the flow path distance to the stream network.

At TCEF, in the beginning of snowmelt only a portion of riparian areas and the drainages of the channel heads contributed to runoff (contributing area $<2\%$), those areas expanded with the onset of melt, activating the "traditional" variable source areas parallel—and close—to the stream network. This is also evident (and especially pronounced in 2007) in the hillslope width functions that indicated an increase in contributing area at distances of less than 300 m from the stream network (Figure 12). However, as opposed to the *Dunne and Black* [1970] variable source areas, the runoff generated at TCEF was almost exclusively subsurface flow. After riparian and near-stream areas became contributing areas, some hillslopes along the stream networked activated and became contributing areas, extending upslope as a function of upslope area, vegetation-mediated ET, and input amount. The increase in contributing area over this period largely occurred up-gradient of the channel heads during this time of maximum connectivity. With snowmelt cessation, many of the hillslope areas fell below the active threshold, leaving only the larger drainages connected. This is demonstrated by hillslope width functions in the transition from 10 to 28 May 2007 (Figure 12, top) and 3 to 17 June 2008 (Figure 12, bottom). The usefulness of changing/dynamic hillslope width functions associated with changing contributing areas was first demonstrated in modeling applications by *Gyasi-Agyei et al*. [1996].

In addition to changing connected area spatial extents and distances from the network, specific watershed runoff source areas have major implications for watershed processes driven or influenced by hydrology and can provide a first approximation of solute source areas and sensitive or more influential areas of watersheds. Knowledge of runoff source areas and how they change through time is critical for deciphering water quantity and composition signals measured at the watershed outlet. For example, the transport of DOC to the stream network [e.g., *McGlynn and McDonnell*, 2003b; *Pacific et al*., 2010] greatly depends on the spatial extent of contributing areas and the intersection of DOC accumulation and connectivity-driven mobilization of DOC to streams. Temporally dynamic streamflow and composition source areas can change in time, even on individual rain event time scales, and may partially explain observed streamflow solute behavior across a range of systems including but not limited to TCEF. However, in addition to just the spatial extent of (saturated) contributing areas, export for certain nutrients, such as DOC, is also dependent on the soil horizon that is being accessed by water in the soil column as well as the onset of flow through preferential pathways—information that is not easily discerned or extracted from WECOH in its current state.

Variable contributing areas and their extent and associated thresholds are likely different for headwater watersheds across geographic regions (see, for example, the compilation of hillslope precipitation thresholds in *Weiler et al*. [2006] or *Ali et al*. [2013]). The importance of the smaller-scale patterns of hillslope to stream connectivity for hydrograph dynamics, however, can change when moving from headwater systems (zero to third order) in a downstream direction to larger river systems (greater than or equal to, e.g., third or fourth order). There can be a shift from hillslope controlled runoff dynamics in headwaters to network and network geometry controlled runoff in larger river systems [e.g., *McGlynn et al*., 2004], thereby obfuscating landscape (hillslope-riparian-stream) connectivity with increasing scale. Obviously, however, headwater watersheds and downstream waters are intrinsically linked [*Alexander et al*., 2007], highlighting the need to better understand how headwaters influence and determine the character of larger river systems [e.g., *Lowe and Likens*, 2005; *Bishop et al*., 2008]. This can become particularly important for assessment of land cover/land use change effects and their mitigation. For example, the effect of harvesting operations and species conversion on the water yield of watersheds has been well documented since the early twentieth century [e.g., *Bates and Henry*, 1928; *Hibbert*, 1967]. However, if increasing water yield with targeted vegetation

removal is desirable, predicting those areas that are larger contributors to streamflow or would become contributors to streamflow with small increases in local storage then becomes a viable model enabled strategy.

Predicting and mapping watershed hydrologic connectivity through time has implications well beyond water quantity. For example, many studies have documented the impact of human-induced land use change in headwater watersheds on water quality [e.g., *Bolstad and Swank*, 1997; *Clinton and Vose*, 2006; *Gardner and McGlynn*, 2009] and have begun to target those changes and landscape locations most influential on downstream water quality [*Gardner et al*., 2011]. Recognizing that the effective watershed is continuously changing, especially during precipitation events, is a first step toward adequately considering landscape hydrologic and runoff generation processes into streamflow composition source attribution. It should be noted however, that documentation of active and connected contributing areas limit the likely water constituent source areas but that these zones themselves do not equally contribute to streamflow composition. Flow path distances to the stream within these connected areas and the threshold change from subsurface to overland flow can offer a next approximation of influence within the contributing areas.

Recognition of the dynamic nature of active and connected watershed areas through time is critical to understanding and managing land and related water resources. Interpretation of observed watershed runoff dynamics and magnitudes in the context of the history of precipitation, its redistribution in the landscape, and how this can influence both base flow and hydrologic response to the next precipitation event is fundamental for landscape and process attribution of observed behavior. Prediction then requires application of well-constrained spatial models consistent with observed processes to estimate landscape hydrological connectivity to stream networks through time and more refined analyses to address particular challenges or questions.

5. Conclusions

Recognizing, understanding, and predicting streamflow source areas through time requires fundamental observations of terrestrial hydrology and influences on water redistribution and storage and efficient numerical representation that is consistent with dominant processes and landscape-scale hydrologic behavior. Here we built on a comprehensive history of detailed spatial and temporal observations of landscape hydrologic connectivity, evapotranspiration, and streamflow to synthesize landscape-scale process observations and understanding with a newly developed parsimonious watershed model. Our approach (WECOH model) includes the combined effects of topographically driven lateral water redistribution and vegetation-mediated evapotranspiration to simulate spatial patterns of watershed water storage through time and streamflow. We calibrated the threshold storage necessary for saturated throughflow and its connectivity across the landscape using empirical observations of water table development (i.e., water table present or not). We calculated active and contributing areas (those active areas hydrologically connected to the stream network) to ascertain and learn from the spatial and temporal evolution of watershed connectivity over the course of two snowmelt seasons. We summarize our findings as follows:

1. Runoff source areas shifted over the course of each melt season from near-stream areas early in the melt progression to lower hillslopes areas and finally areas further up the hillslopes when runoff was concentrated in the larger drainages. With snowmelt recession, the pattern reversed but hysteresis in the pattern was evident, leading to different spatial extent and source areas for streamflow on the rising and falling limbs of the snowmelt hydrograph.
2. The maximum and minimum areas connected to the stream network at any day over the simulation period were 71% and $<1\%$, respectively. Total active area (combination of active, connected and active, disconnected) was always greater than contributing area during the melt seasons but became similar during late summer and winter base flow periods.
3. Over the course of 3 years, 90% of the watershed area was connected for at least one day. The 10% of area that never became connected (above the threshold) to the stream network were either areas with

low upslope accumulated area near ridges or small patches that received little inflows and were interspersed between the more dominant pattern of flow accumulation within the upland drainage network.

The WECOH modeling framework seeks to bridge the gap between knowledge gained from empirical observations and the usefulness of spatially distributed hydrologic models to inform and synthesize understanding at the landscape scale. WECOH is a simple modeling framework to examine how landscape hydrologic connectivity changes over time and how field observations can facilitate the identification of threshold behavior in hydrologic systems. Future research should begin to examine more explicitly the ecohohydrologic feedback between vegetation patterns and landscape-scale patterns of water redistribution, the utility of this framework across landscape settings and climate regimes, and coupled hydrological-biogeochemical representation that includes variable contributing areas for water and solutes.

Appendix A: Snow Melt Model

The snowmelt model was external to the WECOH model and largely followed the steps outlined in *Schaefli and Huss* [2011]. At each 1 hourly time step, the model performed a check to verify an existing snowpack. If there was a snowpack present, the snowpack age, Age_{snow}, was increased by 1 h. The snowpack temperature deficit, T_{def}, was then updated using the average air temperature over a specific, calibrated time in days, t_{snow}. If $Age_{snow} < t_{snow}$, the temperature deficit was calculated over the length of Age_{snow}. Cold content for an existing snowpack was then calculated as:

$$w_c = \frac{c_i}{c_f} h_s (T_{thresh} - T_{def}) \tag{A1}$$

where w_c is cold content in mm, c_i is specific heat capacity of ice (2.06 kJ kg^{-1} °C^{-1}), c_f is latent heat of fusion (334 kJ kg^{-1}), h_s is snow water equivalent (SWE, in mm), T_{thresh} is a temperature threshold for melt (°C), and T_{def} is the snowpack temperature deficit (°C). In case of $T_{def} > 0$, T_{def} was set to 0. Cold content can be considered a heat deficit to overcome before melt begins [*ASCE*, 1996; *Schaefli and Huss*, 2011]. For each time step, a potential melt was then calculated as:

$$M_{pot} = ddf (T_{air} - T_{thresh}) \tag{A2}$$

where ddf is the degree-day factor (mm/°C), T_{air} is air temperature (°C), and T_{thresh} is the threshold temperature (°C) above which melt occurs (calibrated). If $T_{air} > T_{thresh}$, melt abstraction was calculated as:

$$M_{ab} = \min \left[M_{pot}, w_c \right] \tag{A3}$$

In a final step, effective melt was calculated as:

$$melt = \min \left[M_{pot} - M_{ab}, h_s \right]. \tag{A4}$$

Table A1. Calibrated Parameters (Top Part) and Efficiencies (Bottom Part) of the Snowmelt Routine for the 2007 and 2008 Water Years[a]

SWE Calibration	2007	2008
$T_{threshON}$ (°C)	2.9	0.38
$T_{threshST}$ (°C)	4.6	0.66
ddf (mm/h/°C)	0.728	0.208
t_{snow} (days)	178	176
NSE_{ON}	0.98	0.98
NSE_{ST}	0.85	0.99
NSE_{meltON}	0.87	0.88
NSE_{meltST}	0.94	0.93
$Peak_{magnON}$ (mm)	2	14
$Peak_{magnST}$ (mm)	34	11
$Peak_{timeON}$ (h)	13	16
$Peak_{timeST}$ (h)	66	30

[a]*ON* is the Onion Park SNOTEL, *ST* the Stringer Creek SNOTEL, Peak denotes the difference in either peak SWE magnitude or timing between simulated and observed SWE time series).

We included an adjustment for aspect in the snowmelt model so that grid cells that receive more solar insolation were assigned slightly increased melt rates than cells with less solar insolation. For this, we approximated relative potential solar insolation during the spring melt phase (15 March to 15 June) for every grid cell using SAGA GIS, following *Böhner and Antonic* [2009], with default values for the solar constant (1367 W/m^2), height of atmosphere (12,000 m), and vapor pressure (10 mbar). We then calculated mean insolation and assigned all cells within ±10 kWh/m^2 of the mean the value 1. All grid cells with insolation values above or below this range were assigned values greater than or less than 1 based on a linear regression between the mean and maximum and minimum values, respectively. Since the impact of aspect on melt and runoff at TCEF has been found to be much weaker than the elevation effect [*Smith and Marshall*, 2010], the aspect correction was fixed at

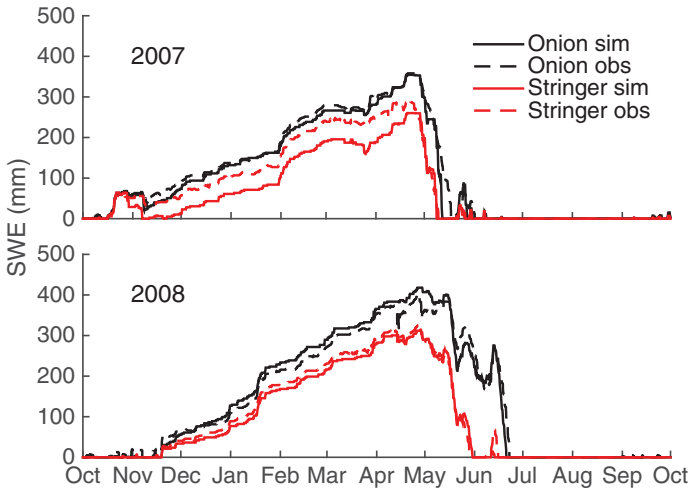

Figure A1. Observed and simulated SWE at the two SNOTEL sites.

5%, i.e., the maximum and minimum values for the insolation correction factor were set to 1.05 and 0.95, respectively. The melt values for each time step were then multiplied by the insolation factor to either increase or decrease snowmelt as a function of aspect. The calibration was not affected by this factor as both SNOTEL sites fall within the range of ±10 kWh/m^2 around the mean insolation. Snowmelt for each grid cell was effectively calculated as:

$$melt_{adj} = melt \times ins, \quad \text{(A5)}$$

where *ins* is the dimensionless insolation correction factor.

Snow accumulation and melt was a simple grid based mass balance of inputs (precipitation, *P*) and outputs ($melt_{adj}$). Small liquid precipitation events during the winter on an existing, thick snowpack further increase the snow water equivalent of the snowpack rather than infiltrate into the soil. To account for those events, we counted liquid precipitation onto an existing snowpack as input to the snowpack when the snowpack had a snow water equivalent ≥50 mm. Change in SWE can be summarized as:

$$\frac{dh_s}{dt} = \begin{cases} \frac{P}{dt}, & \frac{P}{dt} \geq 0 \cap T_{air} < T_{thresh} \\ \frac{P}{dt}, & h_s > 50\,mm \cap T_{air} > T_{thresh} \\ -\frac{melt_{adj}}{dt}, & else \end{cases} \quad \text{(A6)}$$

where *P* is precipitation, h_s is the snowpack water equivalent, $melt_{adj}$ is the modeled melt over the hourly time step, T_{air} is air temperature, and T_{thresh} is the temperature threshold.

For our implementation of the snowmelt model at TCEF, the model contains four calibration parameters: a temperature threshold for each SNOTEL site above which melt occurs and below which precipitation accumulates as snow, $T_{threshON}$ for the Onion SNOTEL site and $T_{threshST}$ for the Stringer SNOTEL site, the degree-day factor that determines how much melt leaves the snowpack at a certain air temperature (*ddf*, identical for both SNOTEL sites), and a parameter that determines the length of the period to approximate snowpack cold content, t_{snow}. Using a 10 m resolution digital elevation model, we calculated precipitation, snow accumulation, and melt for each grid cell on an hourly time step based on observed air temperature and precipitation data from the two SNOTEL sites. Air temperature and precipitation at elevations in between and above the SNOTEL sites were calculated with linear temperature and precipitation lapse rates determined by observed data at the two SNOTEL sites.

The model was calibrated separately for the 2007 and 2008 water years with the observed snow water equivalent (SWE) time series of the Onion Park and Stringer Creek SNOTEL stations (see Figure 1 for locations) and the simulated SWE time series from the two cells that encompass the SNOTEL sites. We calculated Nash-Sutcliffe efficiencies (NSE) for the full SWE time series as well as the main melt period from peak SWE to complete meltout since this period represents the main water input to the ground over the course of the year. Furthermore, we calculated differences in the timing and magnitudes of observed and simulated peak SWE magnitudes for the two SNOTEL sites.

The optimal parameter sets for both years were determined using a four step process. We calculated (1) NSEs for each SNOTEL site for the entire water year, (2) NSEs for each SNOTEL site for the main melt period only (peak SWE till meltout), (3) differences in the magnitudes of peak SWE between simulated and

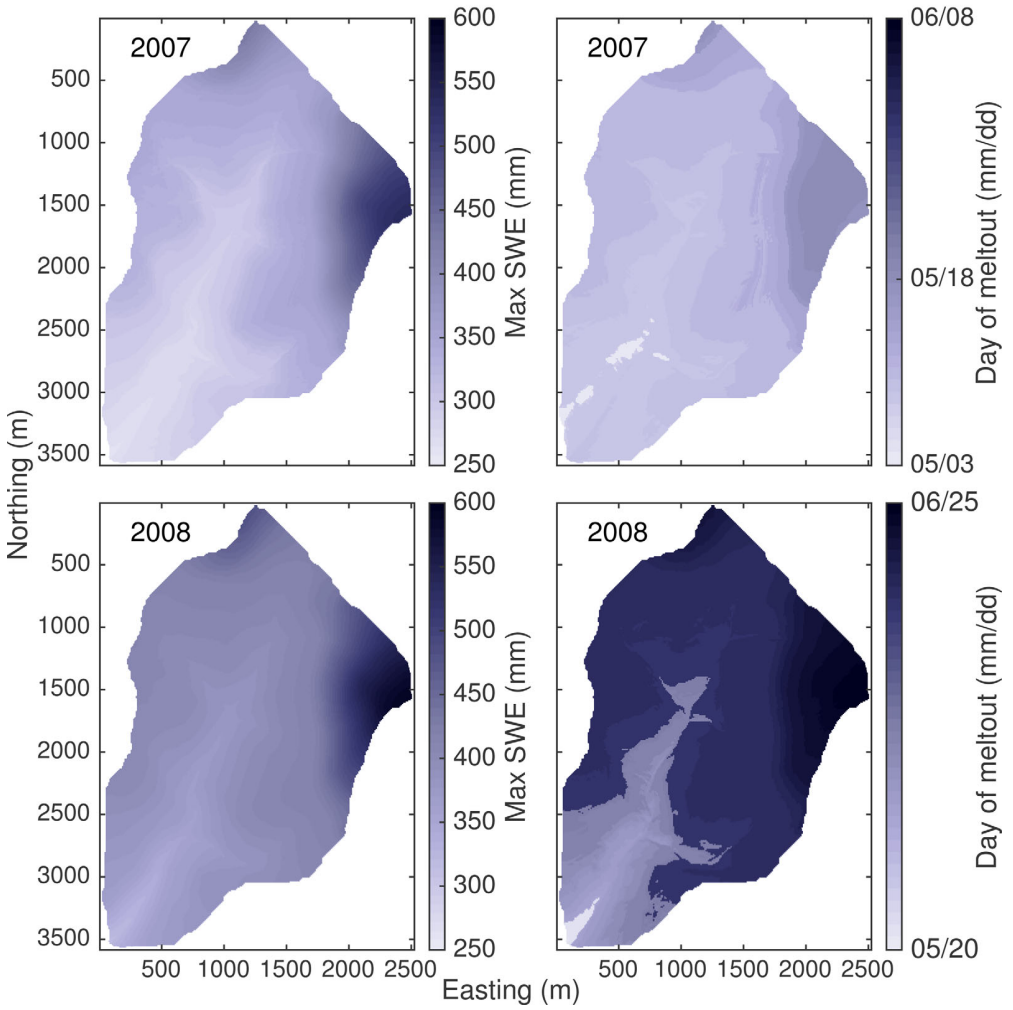

Figure A2. (left column) Maximum SWE accumulation and (right column) day of earliest meltout for the 2007 and 2008 water years. The 18 May is the meltout date for the highest elevation in 2007; for better comparison with the 2008 water year the color scale encompasses the same number of days.

observed SWE time series for each SNOTEL site, and (4) differences in the timing of peak SWE between simulated and observed SWE time series for each SNOTEL site. In a first step, we averaged the NSEs of (1) and took either the 20 best parameter sets or all parameter sets within 2% of the best averaged parameter set (whichever resulted in a smaller subset). In a second step, we averaged the melt-only NSEs of the previously derived subset between the two SNOTEL sites of (2) and chose the 10 parameter sets with the highest averaged melt-only NSEs. In step three, we averaged the differences in peak SWE magnitudes of (3) between the SNOTEL sites and chose the five parameter sets with the minimum combined peak SWE differences. In the final step, we calculated the averaged differences in peak SWE timing of (4) between the SNOTEL sites. The parameter set with the minimum differences in peak timing was the final parameter set for a particular water year. Table A1 and Figure A1 contain the calibrated parameters and efficiencies, and simulated and observed SWE time series, respectively.

We also included an adjustment for aspect in the model so that grid cells that receive more solar insolation were assigned slightly increased melt rates than cells with less solar insolation. For this, we approximated potential solar insolation during the spring melt phase (15 March to 15 June) for every grid cell using SAGA GIS, following *Böhner and Antonic* [2009], using the default values for solar constant (1367 W/m^2), height of atmosphere (12,000 m), and vapor pressure (10 mbar). We then calculated mean insolation and assigned all cells within $\pm$10 kWh/m^2 of the mean the value 1. All grid cells with insolation values above or below this

range were assigned values greater than or less than 1 based on a linear regression between the mean and maximum and minimum values, respectively. Since the impact of aspect on melt and runoff at TCEF was found to be much weaker than the elevation effect [*Smith and Marshall*, 2010], the aspect correction was fixed at 5%, i.e., the maximum and minimum values for the insolation correction factor were set to 1.05 and 0.95, respectively. The melt values for each time step were then multiplied by the insolation factor to either increase or decrease snowmelt based on aspect. The calibration was not affected by this factor as both SNOTEL sites fall within the range of ± 10 kWh/m^2 around the mean insolation.

Sublimation was not automatically accounted for in the snowmelt model. The accumulated sublimation over the course of the winter and spring, as determined by tower latent heat flux, was subsequently subtracted from the postcalibration SWE value of each cell, i.e., when SWE in a grid cell reached the value of sublimation during the melt phase, SWE of that cell was set to 0. The SNOTEL sites are located in open areas, while forested areas in LSC comprise more than 90% of the watershed. The sublimation adjustment therefore partially accounts for increased canopy interception and subsequent sublimation in forests as compared to open areas.

Figure A2 presents the distributed maximum SWE values for the 2007 and 2008 water years, as well as the date of full snowpack ablation for each grid cell. It should be noted that some new snow accumulation took place after the first meltout, especially at lower elevations.

Acknowledgments

This study was made possible by NSF grants EAR-0837937, EAR-0943640, and EAR0337650 to McGlynn, support from Montana State University and Duke University, EAR-0838193 to Emanuel, the 2013 American Geophysical Union Horton Research Grant to Nippgen, and NSF NCALM. The authors would like to thank Kelsey Jencso for discussion and collaboration and the U.S. Department of Agriculture, Forest Service, Rocky Mountain Research Station for access to the site and collaboration. We thank Keith Beven and two anonymous reviewers for constructive feedback that greatly improved the manuscript. Model results (snowmelt as well as rainfall-runoff) and streamflow data can be requested from the first two authors. Streamflow data can also be requested from the USFS. SNOTEL and LIDAR data can be downloaded at http://www.wcc.nrcs.usda.gov/snow/ and http://www.opentopography.org/, respectively.

References

Alexander, R. B., E. W. Boyer, R. A. Smith, G. E. Schwarz, and R. B. Moore (2007), The role of headwater streams in downstream water quality, *J. Am. Water Resour. Assoc.*, *43*(1), 41–59.

Ali, G., C. J. Oswald, C. Spence, E. L. H. Cammeraat, K. J. McGuire, T. Meixner, and S. M. Reaney (2013), Towards a unified threshold-based hydrological theory: Necessary components and recurring challenges, *Hydrol. Processes*, *27*(2), 313–318.

Ambroise, B. (2004), Variable, 'active' versus 'contributing' areas or periods: A necessary distinction, *Hydrol. Processes*, *18*(6), 1149–1155.

ASCE (1996), *Hydrology Handbook*, N. Y.

Band, L. E. (1993), Effect of land-surface representation on forest water and carbon budgets, *J. Hydrol.*, *150*(2–4), 749–772.

Barrett, S. W. (1993), Fire history of tenderfoot creek experimental forest, Lewis and Clark National Forest, report no. INT-92679-RJVA, Intermountain Research Station, Forest Service, U.S.

Bates, C. G., and A. J. Henry (1928), Forest and stream-flow experiment at Wagon WHeel Gap, Colo, Final report on completion of the second phase of the experiment, report no. 30, Monthly Weather Review, U.S. Dep. of Agric.

Betson, R. P. (1964), What is watershed runoff, *J. Geophys. Res.*, *69*(8), 1541–1552.

Beven, K. (2006), A manifesto for the equifinality thesis, *J. Hydrol.*, *320*(1–2), 18–36.

Beven, K. J., and M. J. Kirkby (1979), A physically based, varible contributing area model of basin hydrology, *Hydrol. Sci. Bull.*, *24*, 43–69.

Binley, A., and K. Beven (1992), 3-Dimensional modeling of hillslope hydrology, *Hydrol. Processes*, *6*(3), 347–359.

Bishop, K., I. Buffam, M. Erlandsson, J. Fölster, H. Laudon, J. Seibert, and J. Temnerud (2008), Aqua Incognita: The unknown headwaters, *Hydrol. Processes*, *22*(8), 1239–1242.

Bogaart, P. W., and P. A. Troch (2006), Curvature distribution within hillslopes and catchments and its effect on the hydrological response, *Hydrol. Earth Syst. Sci.*, *10*(6), 925–936.

Böhner, J., and O. Antonic (2009), Land surface parameters specific to topo-climatology, in *Geomorphometry: Concepts, Software, Applications, Dev. Soil Sci.*, vol. 33, edited by T. Hengl and H. I. Reuter, chap. 8, pp. 195–226, Elsevier, Amsterdam, Netherlands.

Bolstad, P. V., and W. T. Swank (1997), Cumulative impacts of landuse on water quality in a southern Appalachian watershed, *J. Am. Water Resour. Assoc.*, *33*(3), 519–533.

Buttle, J. M., and D. J. McDonald (2002), Coupled vertical and lateral preferential flow on a forested slope, *Water Resour. Res.*, *38*(5), doi: 10.1029/2001WR000773.

Buttle, J. M., P. J. Dillon, and G. R. Eerkes (2004), Hydrologic coupling of slopes, riparian zones and streams: An example from the Canadian Shield, *J. Hydrol.*, *287*(1–4), 161–177.

Clinton, B. D., and J. M. Vose (2006), Variation in stream water quality in an urban headwater stream in the southern appalachians, *Water Air Soil Pollut.*, *169*(1–4), 331–353.

Dickinson, W. T., and H. Whiteley (1970), Watershed areas contributing to runoff, in *Results of Research on Representative and Experimental Basins (Wellington Symposium 1970)*, edited, vol. 96, pp. 12–26, IAHS Red Books.

D'Odorico, P., and R. Rigon (2003), Hillslope and channel contributions to the hydrologic response, *Water Resour. Res.*, *39*(5), 1113, doi: 10.1029/2002WR001708.

Dozier, J., and J. M. Melack (1987), Snow deposition, melt, runoff, and chemistry in a small alpine watershed, emerald lake basin, Sequoia National Park, report, Cent. for Remote Sens. and Environ. Opt., Univ. of Calif., Santa Barbara.

Dunne, T., and R. D. Black (1970), Partial area contributions to storm runoff in a small New England watershed, *Water Resour. Res.*, *6*(5), 1296–1311.

Emanuel, R. E., H. E. Epstein, B. L. McGlynn, D. L. Welsch, D. J. Muth, and P. D'Odorico (2010), Spatial and temporal controls on watershed ecohydrology in the northern Rocky Mountains, *Water Resour. Res.*, *46*, W11553, doi:10.1029/2009WR008890.

Emanuel, R. E., D. A. Riveros-Iregui, B. L. McGlynn, and H. E. Epstein (2011), On the spatial heterogeneity of net ecosystem productivity in complex landscapes, *Ecosphere*, *2*(7), 86 pp.

Emanuel, R. E., A. G. Hazen, B. L. McGlynn, and K. G. Jencso (2014), Vegetation and topographic influences on the connectivity of shallow groundwater between hillslopes and streams, *Ecohydrology*, *7*(2), 887–895.

Farnes, P. E., R. C. Shearer, W. W. McCaughey, and K. J. Hansen (1995), Comparisons of hydrology, geology, and physical characteristics between Tenderfoot Creek Experimental Forest (East Side) Montana, and Coram Experimental Forest (West Side) Montana, *Final Rep. RJVA-INT-92734*, 19 pp., USDA For. Serv., Intermountain Res. Stn., Forest. Sci. Lab., Bozeman, Mont.

Fedora, M. A., and R. L. Beschta (1989), Storm runoff simulation using an antecedent precipitation index (Api) model, *J. Hydrol.*, *112*(1–2), 121–133.
Gardner, K. K., and B. L. McGlynn (2009), Seasonality in spatial variability and influence of land use/land cover and watershed characteristics on stream water nitrate concentrations in a developing watershed in the Rocky Mountain West, *Water Resour. Res.*, *45*, W08411, doi:10.1029/2008WR007029.
Gardner, K. K., B. L. McGlynn, and L. A. Marshall (2011), Quantifying watershed sensitivity to spatially variable N loading and the relative importance of watershed N retention mechanisms, *Water Resour. Res.*, *47*, W08524, doi:10.1029/2010WR009738.
Gyasi-Agyei, Y., F. P. deTroch, and P. A. Troch (1996), A dynamic hillslope response model in a geomorphology based rainfall-runoff model, *J. Hydrol.*, *178*(1–4), 1–18.
Hewlett, J. D. (1974), Letters relating to role of subsurface flow in generating surface runoff: 2. Upstream source areas by freeze, R.A., *Water Resour. Res.*, *10*(3), 605–607.
Hewlett, J. D., and A. R. Hibbert (1963), Moisture and energy conditions within a sloping soil mass during drainage, *J. Geophys. Res.*, *68*(4), 1081–1087.
Hewlett, J. D., and A. R. Hibbert (1967), Factors affecting the response of small watersheds to precipitation in humid areas, in *Forest Hydrology*, edited by W. E. Sopper and H. W. Lull, pp. 275–291, Pergamon, Oxford, U. K.
Hibbert, A. R. (1967), Forest treatment effects on water yield, in *Forest Hydrology*, edited by W. E. Sopper and H. W. Lull, pp. 527–543, Pergamon, N. Y.
Holdorf, H. D. (1981), *Soil Resource Inventory, Lewis and Clark National Forest—Interim In-Service Report, On file With the Lewis and Clark National Forest*, For. Supervisor's Off., Great Falls, Mont.
Hood, E., M. Williams, and D. Cline (1999), Sublimation from a seasonal snowpack at a continental, mid-latitude alpine site, *Hydrol. Processes*, *13*(12–13), 1781–1797.
Hwang, T., L. E. Band, J. M. Vose, and C. Tague (2012), Ecosystem processes at the watershed scale: Hydrologic vegetation gradient as an indicator for lateral hydrologic connectivity of headwater catchments, *Water Resour. Res.*, *48*, W06514, doi:10.1029/2011WR011301.
Istanbulluoglu, E., T. Wang, O. M. Wright, and J. D. Lenters (2012), Interpretation of hydrologic trends from a water balance perspective: The role of groundwater storage in the Budyko hypothesis, *Water Resour. Res.*, *48*, W00H16, doi:10.1029/2010WR010100.
Jencso, K. G., and B. L. McGlynn (2011), Hierarchical controls on runoff generation: Topographically driven hydrologic connectivity, geology, and vegetation, *Water Resour. Res.*, *47*, W11527, doi:10.1029/2011WR010666.
Jencso, K. G., B. L. McGlynn, M. N. Gooseff, S. M. Wondzell, K. E. Bencala, and L. A. Marshall (2009), Hydrologic connectivity between landscapes and streams: Transferring reach-and plot-scale understanding to the catchment scale, *Water Resour. Res.*, *45*, W04428, doi:10.1029/2008WR007225.
Jencso, K. G., B. L. McGlynn, M. N. Gooseff, K. E. Bencala, and S. M. Wondzell (2010), Hillslope hydrologic connectivity controls riparian groundwater turnover: Implications of catchment structure for riparian buffering and stream water sources, *Water Resour. Res.*, *46*, W10524, doi:10.1029/2009WR008818.
Kavetski, D., and M. P. Clark (2011), Numerical troubles in conceptual hydrology: Approximations, absurdities and impact on hypothesis testing, *Hydrol. Processes*, *25*(4), 661–670.
Keane, R. E., E. D. Reinhardt, J. Scott, K. Gray, and J. Reardon (2005), Estimating forest canopy bulk density using six indirect methods, *Can. J. For. Res.*, *35*(3), 724–739.
Kelleher, C., T. Wagener, and B. L. McGlynn (2015), Model-based analysis of the influence of catchment properties on hydrologic partitioning across five mountain headwater subcatchments, *Water Resour. Res.*, doi:10.1002/2014WR016147, in press.
Lehmann, P., C. Hinz, G. McGrath, H. J. Tromp-van Meerveld, and J. J. McDonnell (2007), Rainfall threshold for hillslope outflow: An emergent property of flow pathway connectivity, *Hydrol. Earth Syst. Sci.*, *11*(2), 1047–1063.
Lowe, W. H., and G. E. Likens (2005), Moving headwater streams to the head of the class, *BioScience*, *55*(3), 196–197.
McDonnell, J. J. (1990), Rationale for old water discharge through macropores in a steep, humid catchment, *Water Resour. Res.*, *26*(11), 2821–2832.
McGlynn, B. L., and J. J. McDonnell (2003a), Quantifying the relative contributions of riparian and hillslope zones to catchment runoff, *Water Resour. Res.*, *39*(11), 1310, doi:10.1029/2003WR002091.
McGlynn, B. L., and J. J. McDonnell (2003b), Role of discrete landscape units in controlling catchment dissolved organic carbon dynamics, *Water Resour. Res.*, *39*(4), 1090, doi:10.1029/2002WR001525.
McGlynn, B. L., J. J. McDonnell, J. Seibert, and C. Kendall (2004), Scale effects on headwater catchment runoff timing, flow sources, and groundwater-streamflow relations, *Water Resour. Res.*, *40*, W07504, doi:10.1029/2003WR002494.
McGuire, K. J., and J. J. McDonnell (2010), Hydrological connectivity of hillslopes and streams: Characteristic time scales and nonlinearities, *Water Resour. Res.*, *46*, W10543, doi:10.1029/2010WR009341.
McNamara, J. P., D. Chandler, M. Seyfried, and S. Achet (2005), Soil moisture states, lateral flow, and streamflow generation in a semi-arid, snowmelt-driven catchment, *Hydrol. Processes*, *19*(20), 4023–4038.
Mitchell, S. R., R. E. Emanuel, and B. L. McGlynn (2015), Land-atmosphere carbon and water flux relationships to vapor pressure deficit, soil moisture, and stream flow, *Agric. For. Meteorol.*, 208, 108–117.
Molotch, N. P., P. D. Blanken, M. W. Williams, A. A. Turnipseed, R. K. Monson, and S. A. Margulis (2007), Estimating sublimation of intercepted and sub-canopy snow using eddy covariance systems, *Hydrol. Processes*, *21*(12), 1567–1575.
Montgomery, D. R., and W. E. Dietrich (1992), Channel initiation and the problem of landscape scale, *Science*, *255*(5046), 826–830.
Mosley, M. P. (1979), Streamflow generation in a forested watershed, *Water Resour. Res.*, *15*(4), 795–806.
Nippgen, F., B. L. McGlynn, L. A. Marshall, and R. E. Emanuel (2011), Landscape structure and climate influences on hydrologic response, *Water Resour. Res.*, *47*, W12528, doi:10.1029/2011WR011161.
Pacific, V. J., K. G. Jencso, and B. L. McGlynn (2010), Variable flushing mechanisms and landscape structure control stream DOC export during snowmelt in a set of nested catchments, *Biogeochemistry*, *99*(1–3), 193–211.
Payn, R. A., M. N. Gooseff, B. L. McGlynn, K. E. Bencala, and S. M. Wondzell (2012), Exploring changes in the spatial distribution of stream baseflow generation during a seasonal recession, *Water Resour. Res.*, *48*, W04519, doi:10.1029/2011WR011552.
Penna, D., H. J. Tromp-van Meerveld, A. Gobbi, M. Borga, and G. Dalla Fontana (2011), The influence of soil moisture on threshold runoff generation processes in an alpine headwater catchment, *Hydrol. Earth Syst. Sci.*, *15*(3), 689–702.
Peters, N. E., J. Freer, and B. T. Aulenbach (2003), Hydrological dynamics of the Panola Mountain Research Watershed, Georgia, *Ground Water*, *41*(7), 973–988.
Qu, Y., and C. J. Duffy (2007), A semidiscrete finite volume formulation for multiprocess watershed simulation, *Water Resour. Res.*, *43*, W08419, doi:10.1029/2006WR005752.

Quinn, P. F., K. J. Beven, P. Chevallier, and O. Planchon (1991), The prediction of hillslope flow paths for distributed hydrological modelling using digital terrain models, *Hydrol. Processes*, *5*, 59–79.
Ragan, R. M. (1968), An experimental investigation of partial area contributions, paper presented at Berne Symposium, International Association of Hydrological Sciences (IAHS), General Assembly of Bern, pp. 241–251.
Reynolds, M. W., and T. R. Brandt (2006), Preliminary geologic map of the white sulphur springs 30′ × 60′ quadrangle, Montana, U. S. Geol. Surv., USGS Publications Service Group.
Schaefli, B., and M. Huss (2011), Supplementary material for "Integrating point glacier mass balance observations into hydrologic model identification": Cold content concept to delay melt water production, *Hydrol. Earth Syst. Sci.*, *15*(4), 1227–1241.
Sidle, R. C., Y. Tsuboyama, S. Noguchi, I. Hosoda, M. Fujieda, and T. Shimizu (1995), Seasonal hydrologic response at various spatial scales in a small forested catchment, Hitachi-Ohta, Japan, *J. Hydrol.*, *168*(1–4), 227–250.
Sidle, R. C., Y. Tsuboyama, S. Noguchi, I. Hosoda, M. Fujieda, and T. Shimizu (2000), Stormflow generation in steep forested headwaters: A linked hydrogeomorphic paradigm, *Hydrol. Processes*, *14*(3), 369–385.
Smith, T., L. Marshall, B. McGlynn, and K. Jencso (2013), Using field data to inform and evaluate a new model of catchment hydrologic connectivity, *Water Resour. Res.*, *49*, 6834–6846, doi:10.1002/wrcr.20546.
Smith, T. J., and L. A. Marshall (2010), Exploring uncertainty and model predictive performance concepts via a modular snowmelt-runoff modeling framework, *Environ. Modell. Software*, *25*(6), 691–701.
Tetzlaff, D., C. Soulsby, S. Waldron, I. A. Malcolm, P. J. Bacon, S. M. Dunn, A. Lilly, and A. F. Youngson (2007), Conceptualization of runoff processes using a geographical information system and tracers in a nested mesoscale catchment, *Hydrol. Processes*, *21*(10), 1289–1307.
Troch, P. A., J. A. Smith, E. F. Wood, and F. P. Detroch (1994), Hydrologic controls of large floods in a small basin—Central Appalachian case-study, *J. Hydrol.*, *156*(1–4), 285–309.
Tromp-van Meerveld, H. J., and J. J. McDonnell (2006a), Threshold relations in subsurface stormflow: 2. The fill and spill hypothesis, *Water Resour. Res.*, *42*, W02411, doi:10.1029/2004WR003800.
Tromp-van Meerveld, H. J., and J. J. McDonnell (2006b), Threshold relations in subsurface stormflow: 1. A 147-storm analysis of the Panola hillslope, *Water Resour. Res.*, *42*, W02410, doi:10.1029/2004WR003778.
Tsukamoto, Y. (1963), Storm discharge from an experimental watershed, *J. Jpn. For. Soc.*, *45*, 186–190.
Weiler, M., J. J. McDonnell, I. Tromp-van Meerveld, and T. Uchida (2006), Subsurface stormflow, in *Encyclopedia of Hydrological Sciences*, John Wiley, 10, 112.
Wigmosta, M. S., L. W. Vail, and D. P. Lettenmaier (1994), A distributed hydrology-vegetation model for complex terrain, *Water Resour. Res.*, *30*(6), 1665–1679.
Woods, R. A., and L. K. Rowe (1996), The changing spatial variability of subsurface flow across a hillside, *J. Hydrol. N. Z.*, *35*(1), 51–86.